Separation of CO_2 Using Ultra-Thin Multi-Layer Polymeric Membranes for Compartmentalized Fiber Optic Sensor Applications

by

Benjamin Davies
B.Eng., University of Guelph, 2011

A Thesis Submitted in Partial Fulfillment
of the Requirements for the Degree of

MASTER OF APPLIED SCIENCE

in the Department of Mechanical Engineering

Supervisory Committee

Separation of CO_2 Using Ultra-Thin Multi-Layer Polymeric Membranes for Compartmentalized Fiber Optic Sensor Applications

by

Benjamin Davies
B. Eng., University of Guelph, 2011

Supervisory Committee

Dr. Peter Wild (Department of Mechanical Engineering)

Co-Supervisor

Dr. Tom Fyles (Department of Chemistry)

Co-Supervisor

Dr. Martin Jun (Department of Mechanical Engineering)

Departmental Member

Abstract

Supervisory Committee

Dr. Peter Wild, Department of Mechanical Engineering

Co-Supervisor

Dr. Tom Fyles, Department of Chemistry

Co-Supervisor

Dr. Martin Jun, Department of Mechanical Engineering

Departmental Member

Carbon dioxide sequestration is one of many mitigation tools available to help reduce carbon dioxide emissions while other disposal/repurposing methods are being investigated. Geologic sequestration is the most stable option for long-term storage of carbon dioxide (CO_2), with significant CO_2 trapping occurring through mineralization within the first 20-50 years. A fiber optic based monitoring system has been proposed to provide real time concentrations of CO_2 at various points throughout the geologic formation. The proposed sensor is sensitive to the refractive index (RI) of substances in direct contact with the sensing component. As RI is a measurement of light propagating through a bulk medium relative to light propagating through a vacuum, the extraction of the effects of any specific component of that medium to the RI remains very difficult. Therefore, a requirement for a selective barrier to be able to prevent confounding substances from being in contact with the sensor and specifically isolate CO_2 is necessary. As such a method to evaluate the performance of the selective element of the sensor was investigated. Polybenzimidazole (PBI) and VTEC polyimide (PI) 1388 are high performance polymers with good selectivity for CO_2 used in high temperature gas separations. These polymers were spin coated onto a glass substrate and cured to form

ultra-thin (>10 μm) membranes for gas separation. At a range of pressures (0.14 –0.41 MPa) and a set temperature of 24.2±0.8 °C, intrinsic permeabilities to CO_2 and nitrogen (N_2) were investigated as they are the gases of highest prevalence in underground aquifers. Preliminary RI testing for proof of concept has yielded promising results when the sensor is exposed exclusively to CO_2 or N_2. However, the use of both PBI and VTEC PI in these trials resulted in CO_2 selectivities of 0.72 to 0.87 and 0.33 to 0.63 respectively, for corresponding feed pressures of 0.14 to 0.41 MPa. This indicates that both of the polymers are more selective for N_2 and should not be used in CO_2 sensing applications as confounding gas permeants, specifically N_2, will interfere with the sensing element.

Table of Variables and Abbreviations

Latin Characters		
M		molecular weight
J_i		mass flux of component i
L		coefficient of proportionality - flux
x		unit distance through membrane
R		universal gas constant
T		measured temperature
n		mole fraction
v_i		molar volume of component i
p		pressure at feed or permeant interface
c_i		concentration of component i
x		unit thickness measurement
v_s		polymer specific volume
v_f		polymer free volume
v_o		polymer occupied volume
v_{vdw}		van der Waals volume
K		total number of repeating polymer sub-groups
r		free volume element radius
v_h		free volume element volume
N_h		free volume element concentration
T_g		glass transition temperature
S_i		solubility coefficient
p_i		component partial pressure
c_D		Henry's law 'dissolved' solubility
c_H		Langmuir 'hole-filling' solubility
k_D		Henry's Law constant
c'_H		Langmuir hole-filling capacity constant
b_H		Langmuir hole-filling affinity constant
S^0		solubility pre-exponential factor
m		polymer specific adjustable parameter
E_{Di}		activation energy of diffusion

D_i		diffusion coefficient for component i
D_{0i}		diffusion pre-exponential factor
T_{abs}		absolute temperature
a		adjustable intermolecular contributing factor
b		adjustable interchain repulsion factor
d_i		kinetic diameter of component i
c		activation energy constant
f		adjustable activation energy constant
v_i^*		permeant gas molecular (or diffusion) volume
F_i		temperature independent constant of component i for the gas/polymer system
P_i		Permeability of component i
A_i		component specific permeability constant
B_i		component specific permeability constant
k		permeability correlation front factor
P_{0i}		permeability pre-exponential factor
E_p		activation energy of permeation
m_i		mass of component i
p_{isat}		partial pressure at saturation of component i
j_i		molar flux of component i
$\mathcal{P}_i$		molar permeability of component i
Q_i		permeance of component i
$\dot{V}_{STP,i}$		volumetric flow rate of component i at standard temperature and pressure
A		membrane cross sectional area
h		membrane height
t		spin time
h_0		initial polymer solution height
h^*		transition height between film thinning and evaporation mechanisms
t^*		transition time between film thinning and evaporation mechanisms
k		mass transfer coefficient
$\Phi(w_{s0})$		Henry's coefficient
w_{s0}		initial weight fraction of solvent in the polymer solution
$w_{s\infty}^g$		weight fraction of the solvent in the gas phase in an infinite atmosphere

D_a		diffusion coefficient of the polymer solvent in air
v_a		viscosity of air
C		Schmidt number dependent constant
Sc_{air}		Schmidt number
h_f		final film thickness
I		current
E		potential
R_x		resistance for resistor x
l_x		thickness of membrane layer x
R_{irr}		irreversible fouling resistance
R_r		reversible fouling resistance
Greek Characters		
μ		chemical potential
γ		activity coefficient
ρ		density
ε/k		Lennard-Jones potential well-depth parameter
γ_{FVE}		Free volume element overlap factor
γ_n		group-gas pair contribution factor
β		group specific parameter for glassy polymers
γ_{i0}		activity coefficient for component I at the feed stream membrane interface
α_{ij}		selectivity of component I over component j
ρ_p		polymer density
ω		spin rate
η_0		initial polymer viscosity
η		shear-dependent viscosity coefficient
ρ_{sol}		solvent density
Subscripts		
i		component i
j		component j
l		distance through membrane in direction of permeant travel
m		parameter relating specifically to the membrane
Superscripts		
n		Robeson upper bound line slope
Abbreviations		
CO_2		Carbon Dioxide
CH_4		Methane

H_2		Hydrogen
O_2		Oxygen
N_2		Nitrogen
MF		Microfiltration
MV		Macrovoid
UF		Ultrafiltration
NF		Nanofiltration
RO		Reverse Osmosis
ED		Electrodialysis
GS		Gas Separation
PV		Pervaporation
FVE		free volume element
FFV		fractional free volume
PVC		poly(vinyl chloride)
DOP		dioctyl phthalate
CPU		carboxylated polyurethane
HP		high performance
PBI		Polybenzimidazole
DMAc		dimethylacetamide
NMP		N-methyl-2-pyrrolidone
PI		polyimide
LPFG		long period fiber grating

Table of Contents

List of Tables

List of Figures

Acknowledgments

I would like to express my gratitude to my fellow researchers and graduate students (past and present) in the Optical Sensors Research Lab. Your insight and critical thinking helped me get through many road blocks. To Luis Melo for providing a productivity benchmark to follow for each of our weekly meetings. To Geoff Burton and Stephen Warwick for helping to create and troubleshoot my various testing rigs, membrane curing apparatuses, membrane coating chucks, and just generally being hard-working, easy going guys. To Devon Bouchard for showing me that success is not measured solely by the outcome of the project but by determination and commitment.

Dedication

This thesis is dedicated to my parents who provided an endless amount of support, encouragement, and love and to my brother, Ian, and close friends (in no particular order) Adrian, Logan, Ben, Cam, and James who helped me keep my head up through the most difficult parts of life outside the lab.

Chapter 1: Introduction

The research presented in this work is focused on sourcing and testing polymer membranes for the explicit purpose of separating carbon dioxide (CO_2) from both gaseous and aqueous mixtures under low pressures and moderate temperatures. Polymers are comprised of high molecular weight components that are built from a fixed number of repeating base units known as monomers [1]. It is part of a larger, multi-university project focused on creating a fiber-optic based CO_2 sensor (CO_2 optode) for the detection of subsurface CO_2 emissions localized in the vicinity of geological CO_2 sequestration sites. This research has been focused on the development of a polymeric membrane that separates CO_2 from various geological fluids and gases for optical based detection and methods to investigate the membrane selectivity under conditions that are relevant to the intended application. The specifics on the type of optode employed for detection will not be addressed. As many of the existing optical detection methods are inherently non-selective when used independently, a robust method to separate the intended target species (CO_2) is needed. As the amount of CO_2 sent into the atmosphere from the flue gas of an increasing number of industrial point sources continues to rise, mitigating solutions such as sequestration are rapidly developing and being implemented. The compartmentalized sensing component is intended to provide a method of monitoring sequestration sites throughout the initial years of storage to confirm that the storage will be secure.

This chapter will provide information pertaining to the intended area of application for the proposed fiber-optic sensor. Environmental conditions expected at

both shallow and deep locations sub-surface will be introduced as factors affecting the final material selection and aiding in the formation of the project specific objectives prior to presenting the overall organization of this thesis.

1.1 CO_2 Storage and Monitoring

Management and mitigation technologies used to reduce the amount of greenhouse gases released into the atmosphere are being developed side by side in an effort to improve the overall efficiency of large point sources of CO_2 and gradually move to more sustainable non-fossil energy sources. Storage of CO_2 using various reservoirs, such as depleted gas fields, deep ocean, aquifers, and solid carbonate minerals has been proposed [2]. Storage in deep geologic formations is one of the more secure options for storage however, the potential for significant leakage over the course of several hundred years as well as more immediate changes to the structure of the reservoir could lead to a significant loss of CO_2 and subsequent release to the atmosphere [3].

Current geophysical monitoring methods can provide insight into the overall structure of an injection well and overlying rock formations, and they allow for the monitoring of the reaction of the cap rock during the injection [4]. Few methods have been introduced that directly monitor the propagation of CO_2 within the reservoir and/or the surrounding subsurface environment and even fewer are able to provide immediate measurements. These methods are inherently limited as they require either the direct sampling or indirect measurement extrapolation to acquire data.

For the storage of CO_2, a target depth of 800m below the surface is used as the hydrostatic pressure and ambient temperature exceeds its critical point where CO_2 exists as a supercritical fluid [5]. Thus, the mathematical modeling of the chemical interaction between CO_2 and the reservoir solution has been investigated in depth to better understand the ability for CO_2 to be stored under various geologic conditions and to better predict its behaviour once injected [5–12].

Once within the reservoir, two methods of trapping are the most prevalent for successful storage: hydrodynamic and mineral trapping [5]. Hydrodynamic trapping involves the injection of CO_2 into a stable deep aquifer, at a pressure below the fracture pressure, where it is able to travel in a natural flow regime, sitting on top of the formation waters within the reservoir. Over time, the CO_2 will be dissolved and travel by diffusion, dispersion, and convection throughout the aquifer. This occurs over a geological time-scale [5]. The trapping occurs as the CO_2 dissolves into the waters and disperses through diffusion. Mineral trapping refers to geochemical reactions that take place between the feldspars and clays that are present in the aquifer walls and the CO_2 in solution [5]. Immobilization of the CO_2 will also occur where the CO_2 becomes permanently fixed as carbonate minerals, calcite ($CaCO_3$), dolomite ($CaMg(CO_3)_2$), and siderite ($FeCO_3$) [5], [14]. The remaining CO_2 stays physically trapped by the rock surrounding the reservoir. The chemical composition of the water within a reservoir will differ based on geographic location and will contain traces of ions released by the surrounding feldspars and clays affecting salinity and subsequently the reservoirs storage capacity for CO_2 [5], [14].

1.2 Focuses in Membrane Science

In membrane science, structure-function correlations exist to explain two main properties, permeability and permselectivity. The permeability refers to the ability of a membrane to allow passage of a target permeant and relates the molar flux to the driving force. Both the physical properties of the polymer material(s) and the permeant(s) are taken into account when defining the efficiency of a particular membrane-feed interaction. Because the current flux and permselectivity of commercially available polymeric membranes are too low to process the large volumes of various gases that are processed daily in the petrochemical industry, a large portion of membrane separation research is focused on creating an economical solution that yields a low cost membrane with high permeability and permselectivity to the target species [15]. In decades of membrane research with this focus, only 10 different types of polymers are used in commercial gas separations, and none of them were initially designed for this application [15].

1.3 Summary and Project Scope

Efforts, in the literature, have been made to measure the physiochemical properties of both PBI and VTEC PI 1388 using CO_2 and N_2 as permeant species at specific temperatures and pressures to determine their impact on the intrinsic membrane separation qualities. However no work has been completed to measure these characteristics under the conditions that may be experienced when these polymers are cast into a membrane for subsurface environment sensing purposes. Spin coating methods themselves, are not generally considered for these polymers due to their inherent

impracticalities for large scale gas separations. In general, the methods for spinning, heat treating, and subsequently testing ultra-thin (>10 μm) polymer membranes are virtually non-existent in the literature. The aim of the work compiled for this thesis is to provide a well-defined method for producing and testing potential ultra-thin polymeric membranes for gas separations, compile new data for the intrinsic properties of PBI and VTEC PI 1388 at temperatures and pressures that have not been discussed for these substances, and provide a structurally sound method of compartmentalizing a CO_2 optode for subsequent detection and monitoring methodology to be developed.

Chapter 2 of this thesis will review polymeric membrane theory forming a basis from which to compare membrane performance and economics. Chapter 3 outlines the experimental methods to form membranes using the polymers investigated and measure the pertinent membrane properties outlined in Chapter 2. Chapter 4 provides the results of these measurements as well as a short discussion providing implications to current sensor work. Chapter 5 provides conclusions and recommendations for the direction of future research into selective membrane barriers for compartmentalized optode sensing.

Chapter 2: Background and Literature Review

Since the emergence of membrane separation technology in the 1960's, the initial commercialization in the 1970's, and subsequent intensive research effort and serial production of the commercial polymeric membrane was undertaken in the 1980's, membrane-based liquid and gas separation methods have become a more economical solution compared to many commercial separation processes [16]. The improved economics can be attributed to the absence of moving parts in the membrane itself and customizable physical properties that can be developed and tailored to the specific industrial process. While separation efficiency remains a crucial factor in the decision to implement a membrane separation process, low installation and operation costs, and rapidly improving gas selectivity and permeability to specific substances are quickly increasing their attractiveness.

Membrane and polymer material science have grown side by side over the past several decades with each one providing the driving force for the other. The theory behind membrane functionality, on the other hand, needed for the tailoring of membranes through the synthesis and alteration of new and old polymers continues to lag behind new polymer formation and alteration methods [17]. As such, membrane and polymer scientists push to discover new polymers and co-polymers through experimentation in an effort to address specific scientific problems. Research is organized in this manner as the opportunities for the creation of new polymers and subsequent membranes are virtually endless as the novelty lies in the generation of the molecular-level structure. Chemically identical polymers processed in slightly different ways can produce different molecular

scale topographies. Polymers themselves can be blended to improve permeability and permselectivity properties however, the difficulty in this approach lies in discovering polymers that are miscible and show an improvement in the desired properties [17]. Permeability is the measure of the ease with which a specific gas permeant is transported through the membrane material and permselectivity is the ratio of permeabilities of the permeants in a binary mixture [18]. There are many formation procedures for membranes based on variations in cure temperature, polymer concentration, formation method, etc. All of these factors affect the final porosity, mechanical strength, thickness, as well as a number of other physiochemical properties. Because of this, experimental verification of properties reported in the literature is warranted, and most times required, to confirm membrane behaviour [16].

2.1 Membrane-Based Separation

A membrane, in its most ideal form, is a molecular scale filter that separates a mixture of component i and component j to a pure permeate containing only i or j [18]. The molecular diameter of the permeant is generally no more than 1μm and recycling of the feed stream may be necessary to further improve selection [1], [19]. The term "membrane" covers many different structures formed by various materials with different transport properties. The filtration processes in which a membrane can be implemented use a number of different driving forces to accomplish the separation of specific components [20]. Usually, the feed stream is pressurised to provide a driving force for permeation to occur [18]. However the use of membranes for industrial processes is

inherently more attractive for implementation when the pressurization of the feed and/or permeate streams are achieved at lower pressures [18].

Due to the structural diversity of membranes, the use of membrane-based separation can be both energy efficient and economical for many process applications [20]. Benefits and drawbacks to using a membrane for separating various components from a feed stream are summarised in Table 2.1.

Table 2.1: Benefits and Drawbacks to Using Separation Membranes [1]

Benefits	**Limitations**
Separation can be carried out continuously	Concentration polarisation/membrane fouling
Energy consumption is generally low	Low membrane lifetime
Membrane processes can easily be combined with other separation processes	Generally low selectivity
Separation can be carried out under mild conditions	
Up-scaling is easy	
Membrane properties are variable and can be adjusted	
No additives are required	

Although they are few, the limitations to applying a membrane in a separation process need to be seriously addressed for implementation to be successful. There are four major areas of interest pertaining to the development of membranes for industrial/commercial application [20]. These areas are:

- Separation of molecular and particulate mixtures (gaseous or aqueous);
- The controlled release of active agents;

- Membrane reactors and artificial organs and;
- Energy storage and conversion systems.

Many types of membranes exist and the conditions under which they operate can be tailored to be quite narrow. Although the focus of this research is nonporous, dense polymeric membranes for the purposes of gas separation in sensor applications, the fundamental mathematical framework that governs the selective mass transfer across dense polymeric membranes still applies. Fick's laws of diffusion, Fourier's law of heat conduction, and Ohm's law of electrical conduction are all fundamental to the understanding of membrane-based separation [21]. The desired separation can occur due a difference in pressure, concentration, temperature, and/or electrical potential [22], [23]. However, these driving forces are interrelated and can be analysed on the common basis of chemical potential [15], [19 – 21]. The separation of each component of a mixture is determined by its relative transport rate, diffusivity, and sorptivity (solubility) within the membrane material [19].

2.1.1 Types of Membranes

There are many characteristics that help to define what type of membrane should be used for a specific separation process. Membranes can be thick or thin, their structure can be heterogeneous or homogeneous, their transport characteristics can be active or passive, their materials can be natural or synthetic, and they can be neutral or charged [1]. An important first distinction is that membranes can be either biological or synthetic and this work focuses on the latter [1]. Synthetic membranes can be solid or liquid and can be organic or inorganic, each with their inherent advantages and disadvantages for a given

separation process. Organic membranes are typically polymeric whereas inorganic membranes can be produced from metallic oxides, carbon, silica, metals, and zeolite [25], [26]. The geometry of a membrane can take the form of a flat sheet, spread to the desired size and shape, or a tube, generally with a diameter of 1 to 2 cm [20]. Membrane tubes can also be produced as capillaries, with diameters of 200 to 500 μm, or as hollow fibers with a diameter of less than 80 μm [20]. Here, the focus is on solid, flat, polymeric membranes (henceforth referred to as membranes).

The internal structure of a membrane can be dense or porous and this is a major classification that defines the type of transport theory used in modeling the membrane's separation characteristics [1], [25]. More specifically, membranes can be categorized according to their method of production, final working geometry, or bulk structure (isotropic/symmetric or anisotropic/asymmetric) which relates to the size and spacing of its pores [26]. The separation properties of a membrane, which are largely based on its bulk structure, can also be used in its classification. Further sub-classification, based on membrane material, is necessary to fully define the membrane's function and end use.

2.1.2 Physical properties

For the given application, a membrane's mechanical stability, tolerance to feed stream components, tolerance to potential temperature variations, and ease and cost of manufacturing must also be considered when an appropriate membrane is selected [26]. As the drive for membrane innovation is largely based on the separation of various target species in flue gas streams from large point sources, a large portion of the literature focuses on qualities that apply to this industry. Therefore, this review for sensor

applications of membranes is based on analyses developed for large scale gas separations. For industrial adoption of any new polymeric membrane for large volume gas separations, many of the physical properties must be maintained over relatively wide temperature (-20°C to 150°C) and pressure (up to 2000 psig) ranges, and the membrane must exhibit these stabilities for long term use [26]. For the sensor applications targeted here (*i.e.* the detection and quantification of CO_2 in deep underground aquifers), the membrane will not be exposed to such a wide range of operating pressures and temperatures however in using the standard industrial characteristics when evaluating membrane properties for smaller sensor applications, provides a membrane that is more robust. Inevitably, membrane performance will decrease over time due to fouling, swelling, and general degradation, necessitating replacement [26].

To maximize the movement of a specific permeant across a membrane, membrane thickness needs to be minimized, its surface area maximized, and its final structure must accommodate the operating pressures applied. This results in membranes that are susceptible to tear and puncture and require a separate sub-layer to provide external support. Thin flat sheet membranes are often supported with a separate material so that higher feed stream pressures can be tolerated. The support can be cloth (woven or non-woven), the membrane can be stacked in a plate and frame module, or separate non-selective polymers can be used to enhance mechanical stability [27]. The selection of support material does however, depend on the operating conditions for the given process and can cause significant transport resistance when lower flux membranes are used [28].

2.1.3 Membrane Module Configuration and Processes

Two flow configurations for flat membranes are used in both commercial and bench top-scale separation processes, as shown in Figure 2.1.

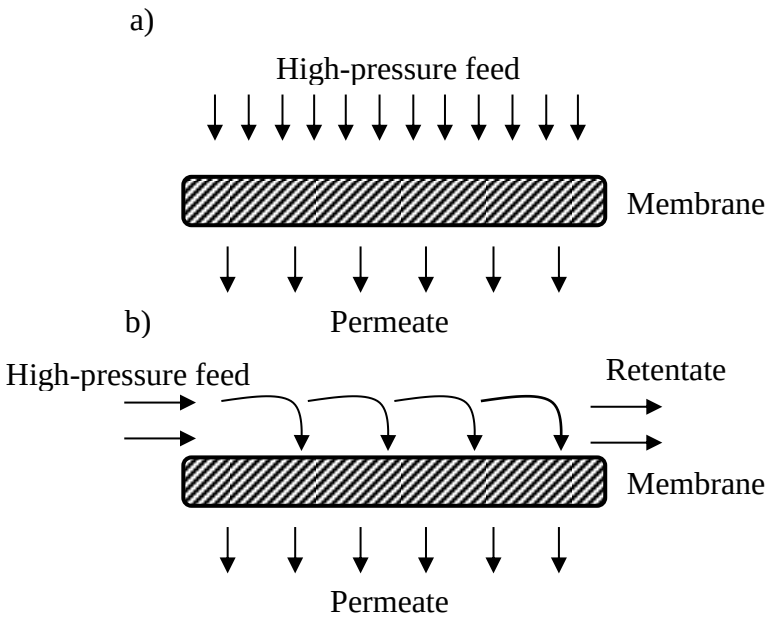

Figure 2.1: a) Dead-end and b) cross-flow membrane flow configurations (adapted from [25]***)***

The dead-end configuration, used mainly in bench top experiments and membrane characterisations, has only the feed and permeate streams. The permeant is forced through the membrane using a pressure or concentration differential in which the permeant follows a gradient from the higher value on the feed side to the lower on the permeate side [25]. The cross-flow configuration allows the permeant to flow parallel to the surface of the membrane. A pressure differential exists across the membrane but a retentate stream is produced [1], [25]. This stream can be used as a product if impurities

are removed from the feed stream by the membrane. Similarly, the permeate stream can be a product stream if a specific component of the feed is desired [1].

2.1.3.1 Membrane Fouling

Both the dead-end and cross-flow configurations for membrane based separations are susceptible to fouling caused by the composition of the feed stream. The resistance of a membrane to flow can be affected by the accumulation of larger particles on the feed surface. There are two types of fouling resistance: irreversible fouling resistance, R_{irr}, that cannot be removed by backwashing of the membrane; and reversible fouling resistance, R_r, that can be reversed by back washing [29]. The values of these resistances are determined empirically using the data from one or more filtration/backwash cycles. Irreversible fouling resistance is calculated from the difference between the total resistance after backwashing and the intrinsic membrane resistance whereas the reversible fouling resistance is the difference between the total resistance before and after backwashing [29]. Generally, membrane fouling is not a large factor in selecting an appropriate membrane for a given application and is addressed after a membrane has been selected based on intrinsic properties using pre-filtration methods to improve the purity of the feed stream.

2.1.3.2 Membrane Processes

There are seven membrane processes that have been applied to industrial scale separations of both gas and liquid permeants. These include microfiltration (MF), ultrafiltration (UF), nanofiltration, (NF), reverse osmosis (RO), electrodialysis (ED), gas separation (GS), and pervaporation (PV) [1], [27], [30]. These processes are defined by

the size of the pores required for the separation of a given permeant and the magnitude and/or type of driving force required. These are summarized in Table 2.2.

Table 2.2: Membrane Processes and their Related Pore Size and Driving Force (adapted from [1], [25], [27]***)***

Membrane Process	Pore Size	Driving Force
Microfiltration	0.05 to 5 μm	ΔP = 0.1 to 3bar
Ultrafiltration	0.005 to 1 μm	ΔP = 0.5 to 5bar
Nanofiltration	0.001 to 0.01 μm	ΔP = 5 to 25bar
Reverse Osmosis	0.0001 to 0.001 μm	ΔP = 10 to 100bar
Electrodialysis		For ionic transport, electrical potential difference, ΔE
Gas Separation		ΔP
Pervaporation		Difference in partial pressure, Δp

The pore size and driving force ranges for each membrane process vary from one author to another. This indicates that instead of an exact point of transition from one membrane process to another, a grey area exists where multiple membrane types could be considered. MF, UF, and NF or RO are all considered *porous* membranes, meaning that any one pore has a fixed location in the membrane's internal structure [25]. ED uses an electrical potential difference to drive ionic permeants across ionic or charged membranes, GS incorporates dense polymeric membranes that follow the solution-diffusion transport mechanism (discussed later in this chapter), and PV separates components from their liquid phase to their gaseous phase [1].

2.1.4 GS Theory

The mechanisms of membrane separation can be described using one of two models: the pore-flow model or the solution-diffusion model. This discrimination is largely based on the size of the particles filtered and the structure of the membrane used. Both models were proposed in the early nineteenth century. However, by the 1980s, the solution-diffusion model was widely accepted as the standard model for RO, PV and, GS membranes [19], [20], [23], [31]. Each model incorporates the concept of free-volume elements (FVEs) which describes the spacing between polymer chains. The solution-diffusion model has pores that fluctuate in volume and position on the timescale of the permeant diffusion and that are much smaller than the relatively large and fixed pores of the pore-flow model. The pore-flow model describes membranes with fixed pores in the 1000 Å (0.1 μm) range [19], [31]. The larger the FVEs, the more likely the pores will exist long enough to produce pore-flow characteristics. The transition between the two models occurs when the FVEs are between 5 and 10 Å in diameter (0.0005 to 0.001 μm) [19], [31].

2.1.4.1 Pore-Flow

The pore-flow model conforms more to the general expectations of filter operation. Separation occurs on the basis of particle size and transport occurs through fixed pores due mostly to a pressure gradient. Larger particles are rejected due to the small pore size [19]. For gas separations, pore-flow separation mechanics can be further divided into three categories based on pore size (displayed in Figure 2.2); convective flow, Knudsen diffusion, and molecular sieving.

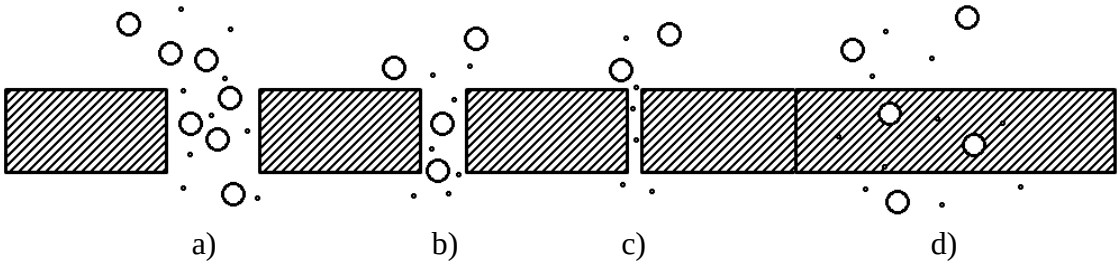

Figure 2.2: Mechanisms for gas separation through porous and dense membranes. a) Convective flow, b) Knudsen diffusion, c) Molecular Sieving, and d) Solution-diffusion. Adapted from [19]**.**

Convective flow occurs if the pores are larger than the gas molecules (from 0.1 to 10 µm) and no separation takes place (Figure 2.2 *a)*) [19]. Knudsen diffusion describes a situation in which the pore diameter is of similar size or smaller than the mean free path of the gas molecules (typically between 5 and 10 Å). Collisions between the molecules and the walls of the filter occur more frequently than between the molecules themselves as the pore size is smaller than the distance a gas molecule would travel in the gas phase between collisions with other gas molecules (Figure 2.2 *b)*) [18], [19]. For pore sizes less than 7 Å (generally used in gas separations) molecular sieving occurs. Here, gas separation can include a combination of both diffusion in the gas phase, through fixed pore channels, and bulk membrane diffusion mechanisms, similar to the solution-diffusion model (Figure 2.2 *c)*) [18], [19].

Graham's law of diffusion governs the pore-flow model dictating that the transport rate for any equimolar gas feed stream is inversely proportional to the square root ratio of the molecular weights, M_i, of the gasses following Equation 2.1 [18], [19].

$$\frac{Rate_1}{Rate_2} = \sqrt{\frac{M_2}{M_1}} \quad 2.1$$

Membranes falling under the pore-flow transport regime are not commercially attractive for most GS operations due to their inherently low selectivity. Only when light gases, such as hydrogen (H_2) and helium (He), require separation from larger gasses is this method viable and surface modification of the filter is generally required [32].

2.1.4.2 Solution-Diffusion

In the solution-diffusion model, gas molecules are transported by making jumps between non-continuous passages that change in size and location based on the motion of polymer chain segments. These transient gaps allow the membrane to be denser and allow for higher permselectivities and smaller permeabilities. Both permeability and permselectivity are further described in sections 2.2.1 and 2.2.3 respectively. The model of this process has three stages. First, the gas dissolves into the face of the membrane that is in contact with the higher pressure, upstream gas. Second, the gas slowly moves through the bulk of the polymer following a concentration and/or pressure difference between feed and permeate streams (the rate limiting step), and finally, desorbs on the permeate side (Figure 2.2 *d)*) [20], [23], [28], [33]. This model assumes that the pressure within the membrane is equal to the applied pressure experienced at the feed side and that the chemical potential gradient across the membrane can be expressed as a concentration gradient or difference in partial pressure [19], [22], [23], [28]. Separation occurs due to differences in solubility of the various chemical species within the membrane material and the rates at which they diffuse through that material [19], [23], [28]. Polymeric gas

separation membranes have no visible pores through which separation occurs. The average pore diameter of these membranes, therefore, must be inferred from the size of the molecules moving through it [19].

2.1.4.3 Flux

To begin to define the solution-diffusion model, it is first assumed that the rates of adsorption and desorption of the permeant at the membrane interface are far greater than its rate of diffusion through the material and that solutions on either side of the membrane are in equilibrium with the membrane material at the interface [23], [28]. This assumption holds for polymeric gas separations but may fail for any separation process involving chemical reactions to facilitate transport or where adsorption is slow [31]. Secondly, it is assumed that the pressure within a dense polymeric membrane is constant at the high pressure value applied to the upstream side of the membrane and that the chemical potential gradient of a permeant can be represented as a concentration gradient alone [23], [31]. In comparison, the driving force gradient within the pore-flow model can be assumed to be represented as a pressure gradient [31].

Gradients of electrical potential, pressure, temperature and concentration are the thermodynamic driving forces of diffusion [1], [23], [31]. It is possible to show a linear relationship that governs the transport due to any of these gradients. However, once two or more components are permeating the membrane simultaneously, coupling phenomena will occur in the fluxes or the forces and non-equilibrium thermodynamics must be employed [1]. Taking the former route, the permeation rate or flux, J(g/cm^2), of a single

component, i, can be reduced to the change in chemical potential, μ, per unit length through a coefficient of proportionality, L . This is represented by Equation 2.2.

$$J_i = -L_i \left(\frac{d\mu_i}{dx}\right) \quad 2.2$$

To simplify the analysis of single component compressible gas diffusion through a polymeric membrane, the driving forces may be further simplified to a function of chemical potential relating pressure and concentration if temperature and electric potential are held constant [23], [31]. The relation to chemical potential, in terms of component i, is displayed in Equation 2.3.

$$d\mu_i = RTd\ln(\gamma_i n_i) + v_i dp \quad 2.3$$

Where γ_i is the activity coefficient linking activity to concentration, n_i is the mole fraction (mol/mol) of component i, v_i is partial molar volume of component i, and p is the pressure. By integrating Equation 2.3 and applying the ideal gas law it can be shown that Equation 2.2 is equivalent to Fick's law of diffusion (Equation 2.4). The steps showing this equivalency are depicted elsewhere [20], [23], [31].

$$J_i = -D_i \left(\frac{dc_i}{dx}\right) \quad 2.4$$

Here, dc_i/dx represents the change in concentration per unit thickness of the membrane and D_i is the diffusion coefficient. This coefficient is a concentration independent measure of the mobility of the molecules within the membrane material and always decreases with increasing size of the molecule [19], [23], [28], [34], [35]. For simplification purposes, this value is implicitly assumed to be constant for each

membrane-permeant interaction. However, for processes in which swelling and plasticization of the membrane occurs due to the permeant, this assumption will be invalid and further analysis of concentration-dependent diffusion and sorption effects will be required [31].

In general, the negative sign for Equation 2.4 indicates the direction of flow moving down the concentration or pressure gradient [19]. Although the individual molecules within the membrane are in random molecular motion, the equation shows that a net transport of matter will occur from the higher concentration to the lower concentration of permeant with a magnitude proportional to the gradient. A more in-depth mathematical analysis can be found in [20], [23], [31]. The aforementioned assumptions and relations for membrane-based gas separations are summarized in Figure 2.3.

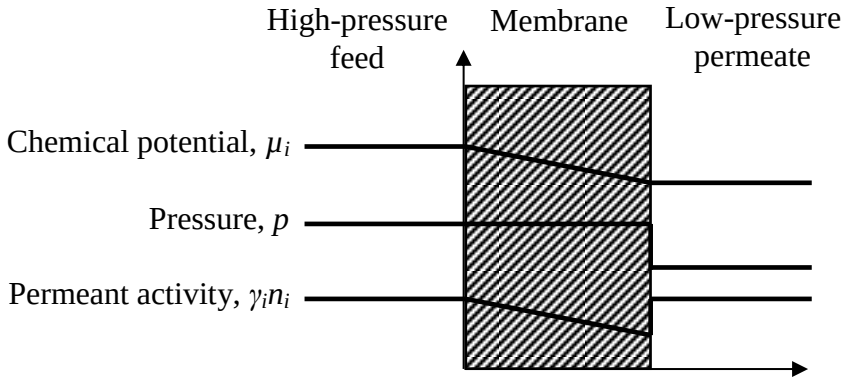

Figure 2.3: Thermodynamic property gradients across a polymeric gas separation membrane that drive diffusion in the solution-diffusion model (adapted from [23]***)***

2.1.5 Transport Properties in GS Membranes

The thermodynamic transport characteristics of GS membranes are the groundwork for understanding the properties of both the membrane and the gases present in the feed stream that drive separation. Using this basis, the measurable properties of a GS membrane will be explained and their impact on membrane selection explored.

2.1.5.1 Polymer Fractional Free Volume

Polymer fractional free volume (FFV) is a well-established measure of the probability of diffusion of a specific permeant across a given membrane. The polymer chains do not pack perfectly as the membrane is cast, due to intermolecular forces present while the membrane is cast, which allows unoccupied space to form. This magnitude and geometry of this space varies from polymer to polymer and can be modified with the addition of side chains to the polymer backbone. The free volume of a polymer is characterized using the formula represented in Equation 2.5 [19], [31], [36]. The FFV is a ratio of the free volume to the polymer's specific volume, $v_s\left(\frac{cm^3}{g}\right) = 1/\rho$ as depicted in Equation 2.6

$$v_f = v_s - v_o \tag{2.5}$$

$$FFV = \frac{v_f}{v_s} \tag{2.6}$$

The occupied volume, v_o, is the sum of the van der Waals radii of the atoms that form the monomer unit which can be calculated using the group contribution method of Bondi or the method provided by Sugden and applied to Equation 2.7 [18], [35–37].

$$v_o = 1.3 \sum_{k=1}^{K} (v_{vdw})_k \quad 2.7$$

The van der Waals volumes of the various groups within the polymer structure are represented by v_{vdw} and K is the total number of groups into which the repeating unit of the polymer structure can be divided (outlined in the literature) [39]. The factor of 1.3 is estimated from the packing densities of crystalline structures at absolute zero and is assumed to apply for all groups and structures within a polymer chain [39]. Molar volumes of various chemical groups that form polymers have been tabulated elsewhere [37], [38]. Typical values for FFV can range from 0.11 to 0.34 [31].

The correlation of FFV to the permeability characteristics of a glassy polymer membrane was presented by Ryzhikh et al. in a more recent paper [36]. A link between the size and connectivity of the FVEs formed in a membrane was explored. The model implies that with the use of the Bondi method for estimating the FFV and measuring the average FVE radius, r, using positron annihilation lifetime spectroscopy probing, one can estimate the mean concentration of FVEs and extrapolate the nature of the changes to transport parameters for a series of polymers under various temperature and pressure conditions. By assuming that the FVEs are spherical, FVE volume, v_h, can be estimated using Equation 2.8 [36].

$$v_h = \frac{4}{3}\pi r^3 \quad 2.8$$

The FVE concentration, N_h, and an understanding of the FVE connectivity, or degree of open porosity, is also required to estimate the FFV according to Equation 2.9 [36].

$$FFV = N_h v_h \quad (2.9)$$

Typically, polymers with a large FFV tend to have a higher porosity [36]. For polymers whose FFV, as estimated using the Bondi method, is within the range of 11-22%, a good linear correlation between the logarithm of permeability ($\log P$) and $1/v_h$ exists [36].

For rubbery polymers, or polymers held above their glass transition temperature, segments of the polymer backbone are allowed to rotate in spaces in its amorphous structure [19]. As the polymer cools below the glass transition temperature, the size of the FFV elements decrease due to the inefficient packing of polymer groups until a point where size restrictions prevent backbone rotation, and the polymer transitions to a fixed state [19]. A relationship between FFV and gas diffusion coefficients can be shown within the specific classes of polymers. By increasing FFV, either during membrane formation or through chemical treatments after the membrane has set, variations in permselectivity and permeability can be achieved [28]. The most desirable membranes have high free volumes and low segmental mobility [18]. Unfortunately, free volume filling of other species in a mixed feed, is a factor in the performance of all membranes.

2.1.5.2 Solubility and Dual Mode Sorption

The solubility coefficient, S, is defined as a measure of the separation that occurs between the upstream gas and the related permeants that have been adsorbed by membrane [34], [35], [40]. The combination of size-based and solubility-based molecular separation yields a “dual mode” sorption mechanism [15]. The sorption, in terms of concentration of gases in rubbery polymers (where temperature, T is greater than the

glass transition temperature, T_g) at low activities, can be simply represented by Henry's law taking the form presented in 2.10 [31].

$$c_i = S_i p_i \tag{2.10}$$

The p_i term is the component specific partial pressure. At higher concentrations, the sorption isotherm becomes convex when plotted against the pressure axis and Equation 2.10 can be rewritten as Equation 2.11 [31].

$$c_i = S(c)_i p_i \tag{2.11}$$

For more condensable gases as well as for most glassy polymer-gas interactions, the concentration of dissolved gas is not a linear function of partial pressure [16], [41]. Rather, a dual mode sorption isotherm is defined using a Henry's law 'dissolved' solubility, c_D, and a Langmuir 'hole-filling' solubility, c_H, as observed in Equation 2.12 [41]. This model is especially applicable to amorphous glassy polymers (i.e. where T < T_g) [31].

$$c_i = c_D + c_H = k_D p_i + \frac{c'_H b p_i}{1 + b p_i} \tag{2.12}$$

Here, k_D is Henry's law coefficient, c'_H is the Langmuir or hole-filling capacity, and b is the Langmuir or hole-filling affinity. The c'_H term is a linear function of the polymer glass transition temperature, T_g, and intercepts the horizontal axis at T_g [16]. The k_D and b terms are both exponential functions of the Lennard-Jones potential well-depth parameter, ε/k [31], [42]. The Henry's law coefficient is described as a limiting value of the solubility coefficient at zero concentration (Equation 2.13) [43].

$$k_D = \lim_{c \to 0} S(c) \tag{2.13}$$

The solubility coefficient can also be correlated to the L-J potential well-depth parameter through Equation 2.14 [31].

$$\log S = \log S^0 + m(\varepsilon/k) \tag{2.14}$$

Here, m has a constant value of approximately 0.01 K^{-1} and S^0 can range from 0.005 to 0.02 cm^3(STP)/cm^3atm depending on the polymer being investigated [31], [42]. Table 3.1 of reference [31] provides some typical gas properties.

2.1.5.3 Diffusion

Diffusion controls the rate at which a permeant moves across a membrane and thus limits the time response of the system. A few attempts to link theoretical computations to the diffusion characteristics of small molecules through polymeric material have been made. A notable contribution to this field was made by Freeman who linked the component specific activation energy of diffusion, E_{D_i}, at temperatures away from the thermal transitions in the polymer (glass transition, melting, etc.), using the Arrhenius Equation (observed in Equation 2.15) [44].

$$D_i = D_{0_i} \exp\left(-\frac{E_{D_i}}{RT_{abs}}\right) \tag{2.15}$$

Here, D_{0_i}, is a pre-exponential factor, R is the universal gas constant, and T_{abs} is the absolute temperature. Freeman employs a simple correlation, often referred to as the 'linear free energy' relation, observed by Barrer and Van Amerongen, that describes the pre-exponential factor [44]. This relation is displayed in Equation 2.16.

$$\ln D_{0_i} = a\left(\frac{E_{D_i}}{RT}\right) - b \qquad 2.16$$

The a term is an intermolecular contributing factor that accounts for interchain repulsion required to permit the passage of the permeant molecule [45]. It has a universal value of 0.64 and is independent of both polymer and gas type [46]. The b term is an intramolecular factor to account for the resistance that the glassy polymer chains have to bending as the permeant molecule passes [45]. It has a value of $-\ln(10^{-4}cm^2/sec) = 9.2$ for rubbery polymers and $-\ln(10^{-5}cm^2/sec) = 11.5$ for glassy polymers and is independent of gas type [47].

The activation energy of diffusion is defined by applying Brandt's model which describes the existence of a finite spacing between polymer chains through which permeant molecules pass [44], [45]. Freeman has modeled E_{D_i} as being proportional to the square of the kinetic or molecular diameter, d_i, (also referred to as the molecular cross section, d_i^2) which characterizes the smallest zeolite pore that a permeant can pass through (Equation 2.17) [44]. Zeolites are crystalline aluminosilicates that have a well-defined repeating pore structure [15].

$$E_{D_i} = cd_i^2 - f \qquad 2.17$$

Both c and f are polymer-specific constants and have been reported by van Krevelen for select polymers based on how high the polymer's diffusivity selectivity is (as described in Section 2.2.3) [44], [47]. The constant, c, can be was reported to be between 250 cal/(mol Å^2), for highly permeable polymers, to 2400 cal/(mol Å^2), for high-performance, glassy polymers [44]. Similarly, f can range from 0 for rubbery polymers

or low-performance glassy polymers to 14,000 cal/mol and is treated as an adjustable parameter [44]. Some common kinetic diameters and molar masses permeant gases are presented in Table 2.3.

Table 2.3: Kinetic (sieving) diameters of common gas permeants [17]

Molecule	H_2	CO_2	O_2	N_2	CH_4
Molar Mass [g/mol]	2.01588	44.0095	31.9988	28.0134	16.0425
Kinetic Diameter [Å]	2.89	3.3	3.46	3.64	3.8

Freeman determined an approximate value of 12,600 cal/mol for f at 298 K for all gas pairs [44]. An approximation of the average spacing between polymer chains can be accomplished using the ratio $\sqrt{f/c}$ [44]. Due to the large number of homogeneous polymers and polymer composites that are potentially viable for a given membrane separation application, a large interest has been placed on correlations relating the transport parameters to the physicochemical properties of polymers in an effort to predict polymer characteristics and efficiency prior to lab-scale testing. However, accurate predictions outside of empirical correlations have yet to be attained.

Most lab scale testing has been conducted at temperatures between 25 and 35°C due to the inherent ease in set up and lower cost in equipment. Because of this, data at low or high operating temperatures is sparse. A study by Yampolskii et al. investigates three prediction models and reports good property correlations for carbon dioxide (CO_2), methane (CH_4), and hydrogen (H_2), depending mostly on the availability of experimental transport data for the given polymer [48].

A more attractive physiochemical property for transport parameter correlation is v_f or FFV (as described in Section 2.1.5.1). This is a well understood property of polymers that directly affects permeation parameters and can be easily obtained [48]. Alentiev and Yampolskii investigated this relation, and similar to Freeman, attempted to fit their prediction to the upper bound line formed by Robeson [49]. This relation is displayed in Equation 2.18.

$$D_i = F_i \exp\left(-\frac{\gamma_{FVE} v_i^*}{v_f}\right) \quad 2.18$$

For this relation, v_i^* is the molar, or diffusion, volume (a constant characteristic for the permeant gas), γ_{FVE} is a parameter to account for free volume element overlap ($0 > \gamma_{FVE} > 1$) and F_i is a temperature independent constant characteristic of the gas/polymer system.

2.1.5.4 Permeability

Park and Paul, building on previous attempts to predict permselectivity, α_{ij}, for various gas pairs using specific functional group (polymer repeat unit structure) contributions, employed FFV as the basis for an analysis of permeability, P_i, as shown in Equation 2.19 [39].

$$P_i = A_i \exp\left(-\frac{B_i}{FFV}\right) \quad 2.19$$

The coefficients A_i and B_i are constants relating to the particular gas. The theoretical approach presented in this paper showed improved fit, relative to the previous approach that utilized Bondi's group contribution method, with experimental data comprising 102

polymers [39]. It is important to note that Park and Paul modified the Bondi method to calculate the occupied volume to account for differences in the size or structure of different gas molecules. This modification to Equation 2.7 is presented in Equation 2.20.

$$(v_o)_n = \sum_{k=1}^{K} \gamma_{nk}(v_{vdw})_k \qquad 2.20$$

The van der Waals volumes can be found in the literature or estimated using the method proposed by Zhao et al. which employs the McGowan characteristic volume [50]. The γ_n values for specific group-gas pairs can be found in Park and Paul's paper [39]. Without knowing the density of the polymer to obtain the specific volume used in Equation 2.5, a relation, presented by van Krevelen, was modified by Park and Paul to estimate this value (Equation 2.21) [39].

$$v_s = \sum_{k=1}^{K} \beta_k(v_{vdw})_k \qquad 2.21$$

Here, β, is a group-specific parameter for glassy polymers.

The group contribution method was also utilized by Robeson et al. who formed an array of equations based on a least squares fit to experimental data [51]. The method was able to accurately predict permeability/permselectivity for the polymers upon which the analysis was based. Predictions were less accurate for polymers outside of the data set. The analysis was based on specific group contributions of the polymer repeat structure and focused mainly on aromatic polymers.

Robeson's empirical upper bound line runs through the points corresponding to the best achieved combination of α_{ij} and P_i [41], [52]. Above this line very few points are able to be realized and this is the area where most of the research today is focused. This relation is presented in Equation 2.22.

$$P_i = k\alpha_{ij}^n \tag{2.22}$$

The relation is logarithmic, the factor, k, is a proportionality constant, and the slope of this line, *n*, correlates with the L-J kinetic diameter difference between gas pairs. This indicates that the separation capabilities of a specific polymeric membrane is largely governed by its diffusion coefficient [41]. The efficiency of the membrane is, therefore, determined by the average pore size and distribution of pores throughout the membrane [41]. The log-log correlation was shown initially to be valid for O_2/N_2, H_2/N_2, He/N_2, H_2/CH_4, He/CH_4, CO_2/CH_4, and He/H_2 and more recently updated to include CO_2/N_2 separations [52].

This approach to modeling membrane permeability is only applicable to membranes of thicknesses up to approximately 1000 Å [41]. Due to the lack of experimental data outside of the 25-35°C range, correlation to higher or lower temperatures has only been estimated using the Arrhenius Equation, where P_{0_i} is a pre-exponential factor and E_p is the activation energy of permeation (Equation 2.23) [31].

$$P_i = P_{0_i} \exp\left(-\frac{E_p}{RT}\right) \tag{2.23}$$

2.2 Measurement of Membrane Properties

The choice of membrane material is crucial to its performance and efficiency in the given application as this choice reflects a trade-off between permeability and permselectivity for the given permeant. Higher permselectivity, is the more desirable of the two, in terms of ideal qualities, as in most cases permeability can be enhanced by altering the membrane thickness and/or composition [49]. Higher permselectivity will yield a more pure product stream whereas higher permeability will reduce capital costs by lowering the surface area requirements to treat a given permeant. The membrane selection process, historically, uses trial and error, typically guided by a team of polymer chemists and physicists having a basis of knowledge of polymer mechanics and physics [28]. Using the permeability and permselectivity relationship presented by Robeson, the potential effectiveness of a membrane can be determined by locating or adding a particular polymer's point on the log-log plot of permselectivity vs. permeability and comparing it to the position of the suggested "upper bound" [52]. Figure 2.4 displays the upper bound correlation for CO_2/N_2 separations.

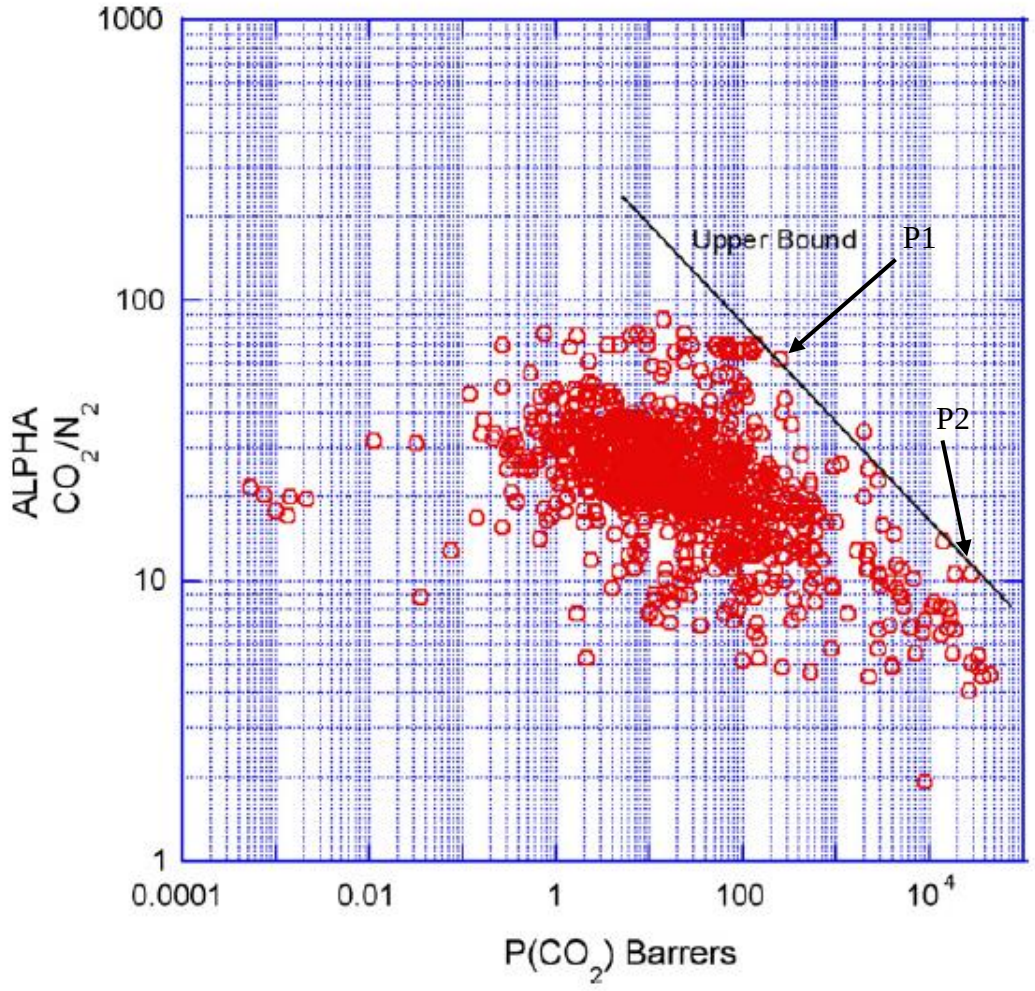

Figure 2.4: Upper bound correlation for CO_2/N_2 separations (from [52]***)***

Displayed in this graph are the limits of close to 300 known polymer membranes able to effectively separate CO_2 from N_2. The highest permselectivity displayed is Poly[bis(2-(2-methoxyethoxy)ethoxy)phosphazene] (P1) with a value of 62.5 corresponding to a permeability of 250 Barrers [52]. The highest permeability is 29000 Barrers corresponding to a permselectivity of 10.7 for Poly(trimethylsilypropyne) (P2) [52]. There are points displayed with either a higher permeability or a higher permselectivity

however as both of these points lie on the upper bound line, these polymers have the highest combination of the two properties.

When there is an option to pre-treat the feed stream, higher expenses associated with exotic, highly permselective material can be avoided [17]. Pre-treatment is a consideration largely applying to the industrial scale membrane separations such as RO, where the removal of aggressive contaminants, such as: gross particulates, humic acids, and silicates, in the feed stream can be a less costly alternative than using premium membrane material [17]. In instances where these contaminants make up a large portion of the feed and can damage membrane material as well as other downstream components, the use of premium membranes is justified. An example of this would be chlor-alkali cells where the feed stream components are very aggressive and the use of Nafion Perfluorinated membranes is necessary [17].

Most of the permeability and permselectivity data published to date has been collected using flat, thick, dense membrane supported by a porous backing to prevent bursting [28]. Any changes in polymer chemistry that alter the solubility or diffusion properties for a specific permeant alter those coefficients in similar ways for the other permeants involved in the separation [19].

2.2.1 Flux, Solubility, and Permeability

The solubility coefficient positively correlates with the size of the permeant, where the larger molecules have higher boiling points, critical temperatures, and L-J parameters due to increased van der Waals interactions with the polymer matrix [28], [31]. For gas phase permeants, this behaviour is as shown in Equation 2.24. The relation

between concentration and partial pressure of the gas at the feed-membrane interface is shown in Equation 2.25. Detailed derivations of these can be found in [23]. A similar relation can be derived for component i at the downstream interface after the permeant has passed through the membrane.

$$S_i = \frac{m_i \rho_m \gamma_{i_0}}{\gamma_{i_{0(m)}} p_{i_{sat}}} \tag{2.24}$$

$$c_{i_{0(m)}} = S_i * p_{i_l} \tag{2.25}$$

The m, represents mass, ρ_m, density of the membrane material, p_i, partial pressure for the specific permeant, and $p_{i_{sat}}$, partial pressure at saturation. The subscripts 0 and l represent the feed and permeate streams, respectively, where l is the total thickness of the membrane. $c_{i_{0(m)}}$ is the concentration of component i within the membrane at the feed-membrane interface. After integration and substitution of Equations 2.24 and 2.25, Fick's law expression for permeant flux is redefined and simplified as a function of gas phase permeability and partial pressures of the feed stream. Flux is now defined as the difference between the partial pressure at the feed-membrane interface p_{i_0}, and permeate-membrane interface, p_{i_l}, over the membrane thickness multiplied by the permeability of component i as shown in Equation 2.26 [23].

$$J_i = \frac{P_i\left(p_{i_0} - p_{i_l}\right)}{l} \tag{2.26}$$

The mobility of a polymer segment or backbone can be traced back to both the intersegmental factors as well as intrasegmental effects due to the presence, or lack of, substituted radical groups or atoms that change the polarity of the attached segment [18]. With increasing polarity of the polymer segment both the intersegmental attraction and the effectiveness of backbone packing become higher. Little or no change in the FFV, lower diffusivity, higher permselectivity, and only minor changes to solubility selectivity can also result [18].

Equation 2.26 is a calculation of a mass flux (g/cm^2·s). It is convention to express this value as a molar flux (cm^3(STP)/cm^2·s) and the conversion to flux can achieved using the ratio of molar volume to mass, as shown in Equation 2.27 [23].

$$j_i = J_i \frac{v_i}{m_i} \tag{2.27}$$

Similarly, the permeability can be converted to molar units (cm^3(STP)·cm/cm^2·s·cmHg), as shown in Equation 2.28.

$$\mathcal{P}_i = P_i \frac{v_i}{m_i} \tag{2.28}$$

More practically, the molar permeability can be quantified as the product of the solubility coefficient (the thermodynamic parameter) and the diffusion coefficient (the kinetic parameter) using Equation 2.29 [19], [23], [28], [40], [53]. For various gases this value can range from 10^{-4} to 10^4 [54].

$$\mathcal{P}_i = D_i S_i \tag{2.29}$$

Commonly, molar permeability is measured in Barrers (10^{-10}cm^3(STP)·cm·cm^{-2}·s^{-1}·cmHg^{-1}), derived from the diffusivity coefficient in cm^{2}s^{-1}. The solubility coefficient is measured in cm^3(STP)cmHg^{-1} and can also be computed using the membrane flux, thickness, and the pressure differential across the membrane as shown in Equation 2.30.

$$\mathcal{P}_i = \frac{j_i \cdot l}{\Delta p_i} \tag{2.30}$$

Fundamentally, permeability is governed by the thermally agitated motion of the chain segments that comprise the polymer matrix that generate permeant-scale transient gaps through which permeants diffuse [18].

2.2.2 Permeance

Another parameter useful in selecting appropriate gas separating membranes, on the basis of performance, is gas permeance (or gas permeation rate), Q. Q can be used as a measure of membrane performance for a specific gas permeant and is a ratio of the molar flux to change in partial pressure of the permeant gas. This relationship is displayed in Equation 2.31.

$$Q_i = \frac{j_i}{\Delta p_i} \tag{2.31}$$

To calculate this value, the molar flux must be measured using the volumetric flow rate of the gas at standard temperature and pressure, $\dot{V}_{STP}$, and the membrane area, A, exposed to the feed gas. This relation is shown in Equation 2.32.

$$j_i = \frac{\dot{V}_{STP,i}}{A} \tag{2.32}$$

Gas permeance is measured in gas permeation units (GPUs), where 1 GPU is 10^{-6}cm^3(STP)·cm^{-2}·s^{-1}·cmHg^{-1}. High flux is desirable for a separation process so that membrane size requirements are reduced for a given flow rate, thus, reducing system costs and improving membrane productivity [26]. This is an important relation as promising membranes for industrial gas separations are prohibitively expensive to manufacture due to their complex chemical makeup and/or manufacturing process. Current research aims to reduce these costs by characterising the gas separation properties of a large number of commercially available polymers using these standard properties.

2.2.3 Permselectivity

It is difficult to improve the permselectivity of a membrane material by more than a factor of two or three as the permselectivity is simply a ratio of one permeability coefficient to another (Equation 2.33) [19].

$$\alpha_{ij} = \frac{\mathcal{P}_i}{\mathcal{P}_i} = \frac{D_i}{D_j} \cdot \frac{S_i}{S_j} \cdot \frac{\Delta p_i / p_{i,feed}}{\Delta p_j / p_{j,feed}} \qquad 2.33$$

The ideal separation factor or permselectivity, α_{ij}, of one gas relative to another includes the product of the ratio of diffusion coefficients and solubility coefficients for the permeating gases which are referred to as the mobility selectivity and solubility selectivity factors, respectively. The mobility selectivity relates to the ability of the polymer matrix to function as a size- and shape-selective membrane based on backbone chain rigidity and intersegmental packing [17]. Solubility selectivity is based on the interactions between permeants and the polymer composing the membrane [17]. For a

gas, the condensability, defined by its critical temperature, correlates positivity with its solubility selectivity [17].

To calculate permselectivity, the driving force term (the final term in Equation 2.33) is included to account for downstream pressures that are not held at vacuum [18]. However, most membrane material screening is carried out under simple conditions in which the downstream pressure is controlled or at atmospheric pressures and thus the driving force factor is sufficiently close to unity to be negligible [18]. More stringent restrictions can be placed on the application of the ideal separation factor (Equation 2.33) however, it is generally accepted that it can be used as a first approximation to focus on other factors of material selection [17]. For the common gases (He, H_2, O_2, N_2) these assumptions hold as both the solubility and diffusion coefficients are functions of neither temperature nor pressure over a large range [41]. This is also true for CO_2 and CH_4 at relatively low partial pressures and modest temperatures [41]. However, for condensable gases, the change in partial pressure may be sufficient to significantly alter the permeability [41]. Complications also arise for CO_2, SO_2, and NH_3 at higher temperatures as their relatively high critical temperatures and tendency to interact with polymers can cause membrane plasticization [17]. Under these conditions, the permselectivity can be lower than expected as the downstream partial pressures for the select permeant gases will not be zero and the diffusion and solubility coefficients will be altered by the membrane plasticization and temperature effects [17]. However, the permselectivity allows for useful comparisons of different material-gas interactions on an equivalent basis.

Membrane performance is more dependent on the selected material, internal membrane structure, membrane configuration within a filtration system, and the overall system design than on the ability to make specific modifications to chemical structure [53]. The permeability and selectivity of a membrane are key factors in determining the economics of the selected membrane material as these parameters are a function of the membrane physical and chemical structure and of the nature of the permeant (*i.e.* size, shape, and polarity) [40], [53]. However, the permeability of a mixture of gases is strongly influenced by operating temperature as solubility and diffusivity for each gas and polymer has a distinct temperature dependence [28]. Thus, membrane thickness, operating temperature, and presence of confounding species in the feed stream, need to be considered when selecting an appropriate membrane [28]. Specifically, condensable, polar, and reactive components alter permeabilities and permselectivities for a given feed mixture. Unfortunately, there is no exact relationship to guide the membrane selection process based on permeability and selectivity data.

2.3 Polymeric Membranes

The degree of polymerization or number of monomer segments in a polymer will increase the molecular weight in proportion to the molecular weight of each repeating unit [1]. Polymer chains can be linked, branched, or crosslinked. Linking refers to the standard polymer formation where monomers are linked end to end. Branching occurs when a separate polymer chain forms off of the primary chain. Crosslinking is usually caused by separate chemical reaction in which two separate polymer chains are connected by a covalent bond [1]. Each polymer chain has a virtually infinite number of formations

once cast, ranging from unfolded to completely folded or coiled, depending on the conditions in which it was formed. This coiling produces inter- and intra-molecular forces that both determine the physical properties of the final polymeric membrane as well as define the transport characteristics for a given permeant.

The two states in which a polymer can exist, being glassy or rubbery, affect its mechanical, chemical, thermal, and permeation properties [1]. Rubbery polymers characteristically allow for higher permeant diffusion due to segments of the polymer backbone being free to rotate around its axis [19]. Glassy polymers allow limited backbone motion resulting in a more rigid membrane with a low permeant diffusion [19]. However, by raising the temperature of a glassy polymer to the point at which the thermal energy is sufficient to overcome the resistance formed by the polymer's inherent chemical structure (*i.e.* the glass transition temperature, T_g), the polymer's bonding structure is altered to allow permeant flow similar to that seen in rubbery polymers [19]. The material chosen for membranes has a direct effect on membrane performance as the size and abundance of pores within the membrane are altered when the glassy or rubbery state is altered based on the operating temperature [1]. To a similar but lesser extent, the material chosen for porous polymeric membranes can be affected by parameters such as chemical and thermal stability and indirectly by surface effects such as adsorption and wettability [1].

Membranes have small pores that, because of the inefficient packing of the polymer, vary in size and location due to inter-molecular forces. Membranes therefore follow a transport regime involving a stage of dissolution and diffusion of the permeant

whereas porous membranes allow transport to occur in the continuous fluid phase which fills the membrane pores [25]. It is well established that the solution diffusion model accurately represents gas transport through this type of polymeric membrane and, therefore, performance enhancements can be achieved by improving diffusion and/or solubility. However, as stated in section 2.2, diffusion or solubility improvement is difficult to achieve individually without one parameter negatively affecting the other. Therefore, the polymer used to make the membrane is crucial to the separation performance.

Key factors used in evaluating the performance and economy of a particular membrane for use in a separation process are selectivity, permeability, flux, and durability [30], [33]. These factors characterise a membrane's physical and/or chemical affinity toward a specific permeant [1]. The ratio of diffusion coefficients for a gas pair is defined as mobility selectivity (the first term in Equation 2.33) [28]. Each diffusion coefficient on its own is a direct measurement of the ability of a polymer to act as a size and shape selective medium [55]. This is because polymer segment mobility, or the freedom that the polymer backbone has to rotate, and inter-chain packing, or how efficiently the polymer chains have packed during membrane formation, together play a more substantial role in determining gas permeability than solubility [55]. The solubility selectivity (the second term in Equation 2.33), or the ratio of solubilities, for a gas pair are more affected by external factors, such as temperature and/or pressure, owing to the fact that the solubility constant follows Henry's law and is related to the boiling and critical points for a given gas [55].

The flux, permeability, and selectivity are largely governed by the effective membrane thickness and the ability of the formation process to achieve “pinhole” and macrovoid (MV) free membranes [33]. These parameters can be finely tuned to achieve more desirable permeabilities through the use of composite membranes, mixed matrix membranes, or modified membranes through radical group substitution. By combining beneficial properties of multiple classifications of membranes, a more efficient and economical solution for a given separation process can be achieved when compared to membranes formed from the basic polymer however, an in depth analysis of this type of membrane specific to gas separations is beyond the scope of this project.

A large number of studies have been undertaken on the industrial, government, and research lab levels to develop membranes that are both more permeable and more selective than first generation materials. Based on an exhaustive review of the literature, a structure-property database for homogeneous gas separating polymeric membranes was formed by Robeson, showing distinctly that polymers that are more permeable are generally less selective and vice versa [16], [52]. An “upper-bound” line was empirically fit to the log-log plots of selectivity versus permeability of gas pairs, and subsequently updated [16], [52]. All of the data points collected, for both papers, involved a similar membrane formation procedure. Heterogeneous membranes were left out of this analysis as the number of combinations that could be fabricated to surpass the current upper bound would be far too great to easily display. Polymer modifications aimed at surpassing this upper bound use the addition of bulky groups that tend to kink the

polymer backbone which inhibits backbone rotation and disrupts interchain packing (increasing FFV) [17].

2.3.1 Low selectivity polymers

Polymers selected for their inherent low selectivity and high permeability are ideal candidates for the caulking material used to fill MV's and pin holes. As most polymers, once cast into membranes, show preference for certain permeants over others, the addition of plasticizers can help to shift the balance of permeability and permselectivity. Ideally, these polymers will initially have the highest permeability to the permeants that are desired to be separated.

2.3.1.1 Polyvinyl Chloride

Poly(vinyl chloride) (PVC), the chemical structure of which is displayed in Figure 2.5, is a robust, highly available, low cost glassy polymer (at ambient conditions) that, once cast into a membrane, has good mechanical strength and above average acid, alkali, and solvent resistance [29].

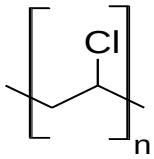

Figure 2.5: Chemical Structure of poly(vinyl chloride) mainly used in UF as a pre-treatment for RO [29]

Unmodified PVC characteristically has a low permeability, high selectivity polymer however, as the polymer has an especially high compatibility with additives, numerous

authors have functionalized and modified the base PVC structure in an effort to improve its permselectivity [56–60]. With the addition of dioctyl phthalate (DOP) the gas permeability can be significantly increased and selectivity reduced. Lim et al. observed an increasing exponential-like trend in the enhancement of $\mathcal{P}_{CO_2}$ for a carboxylated polyurethane (CPU)/carboxylated PVC blended membrane for increasing amounts of DOP [60]. This trend was linked to an increase in the free volume which is in accordance to the permeability models presented by Park and Paul for glassy polymers [39], [60].

2.3.2 High-performance polymers

High-performance (HP) polymers possess a number of beneficial properties that allows them to function in many extreme environments. HP polymers however, are used mainly for advanced composites and for fabricating electronic components [61]. HP polymers possess high mechanical strength, compression strength, stiffness, good chemical resistance, low water absorption, and maintain their properties at highly elevated temperatures [61]. Generally, these characteristics all relate to glassy polymers. HP polymers are also attracting attention for use in high temperature gas separations from mixed-gas streams, pushing the upper bound limit suggested by Robeson. The high T_g (>150°C) and aromatic back bones of these polymers help to limit the interactions of the polymer matrix and the permeating gas [15]. These polymers are well suited for gas separations at higher temperatures due to higher permeabilities. However, the permeability/permselectivity trade-off at higher temperatures indicates that they are also slightly less selective than their non-HP polymer counterparts.

2.3.2.1 Polybenzimidazole

Polybenzimidazole (PBI), also known as Celazole or poly(2,2'(*m*-phenylene)-5,5'-bis-benzimidazole), is a high molecular weight, HP polymer, that can withstand prolonged exposure to strong acids, bases, and high temperature without degradation [62]. It is not soluble in most organic solvents and only partially soluble in dimethylacetamide (DMAc) or N-methyl-2-pyrrolidone (NMP) [63]. Due to these robust properties, it has been tested for a large number of applications in harsh environments [64].

PBI consists of a hydrogen bonded network that tightens the polymer backbone structure. This network yields a densely packed internal structure and high backbone rigidity [64]. The stability of the hydrogen bonds are largely affected by the external temperature and how close that temperature is to the T_g. PBI shows a high selectivity for H_2 over CO_2 at high pressures and temperatures (*i.e.* > 300°) [55], [64]. At lower temperatures (*i.e.* <50°), the H_2/CO_2 selectivity is much lower as their permeabilities are similar stemming from a tighter backbone structure [55]. At 25°C, permeabilities of 0.09 and 0.01 Barrers were observed whereas, at 340°C, permeabilities of 18 and 4 Barrers were observed, for H_2 and CO_2 respectively [55]. PBI, over all, has a low gas permeability when compared to permeabilities noted by Robeson on the upper bound line. Due to this, low membrane gas fluxes are expected and may be difficult to quantify at lower temperatures [64]. The monomer unit of polybenzimidazole is shown in Figure 2.6.

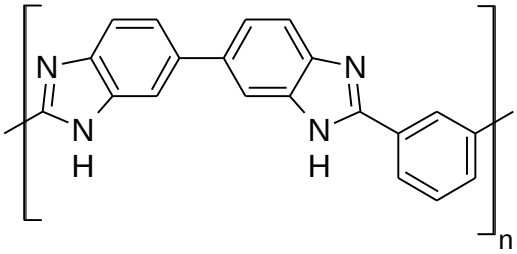

Figure 2.6: Chemical Structure of poly(2,2'-(m-phenylene)-5,5'-bibenzimidazole) mainly used in hyperfiltration membranes [65]**.**

2.3.2.2 VTEC Polyimide

A series of proprietary polyimides (PIs), under the trade name "VTEC", use polyamic acids functionalized with different chemical groups to allow them to be more soluble in organic solvents [63]. The imide monomer unit is displayed in Figure 2.7.

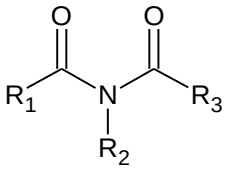

Figure 2.7: Imide monomer structure. R_1, R_2, and R_3 are structures specific to the polymer and desired membrane properties. Usually, R_1 and R_2 are carbon atoms of an aromatic ring.

The VTEC group of PIs has only recently become commercially available in multi-gallon quantities and, as a result, the chemical structures and chemical properties remain a trade secret. At room temperature, PIs have intersegmental packing which causes reductions in the mobility of the polymer backbone leading to higher permeability and selectivity [55]. Being a HP polymer, they are also able to remain stable for high temperature gas separations, having a thermal decomposition temperature > 500°C and

very small dimensional changes when heated to 400°C [63]. Once cast into membranes, these polymers show attractive gas separations at temperatures around 250°C [63].

2.4 Methods of Forming Polymeric Membranes

There are a large number of formation methods for creating membranes. Each of these methods has a permanent effect on the transport properties of the final membrane. The most important method for creating non-porous membranes consists of two stages. First, the polymer-solvent mixture is coated on an appropriate substrate then a phase inversion technique is implemented to create the self-supporting membrane structure [1].

2.4.1 Manual Casting

A polymer membrane can be manually cast on a flat substrate using a casting knife, or doctor blade, to spread the polymer to a prescribed thickness. The resulting membrane will have a reduced thickness due to solvent evaporation, typically in the range of 50 – 150 μm [1]. As the tool used for this is operated manually, sources of error arise that bring into question the uniformity of the membrane and the ability to predict the final membrane thickness accurately.

2.4.2 Spin Coating

Spin coating or spin casting is a well-known process in the microelectronics industry. In this process, liquid polymer is applied to a spinning planar substrate. The thickness of the resulting membrane can be less than 50 μm, limited only by the mechanical strength of the polymer during and after removal from the substrate. The

resulting membrane thickness is governed primarily by centrifugal effects. This process can be used in place of casting to achieve thinner membranes. Figure 2.8 displays the four stages of the spin coating process.

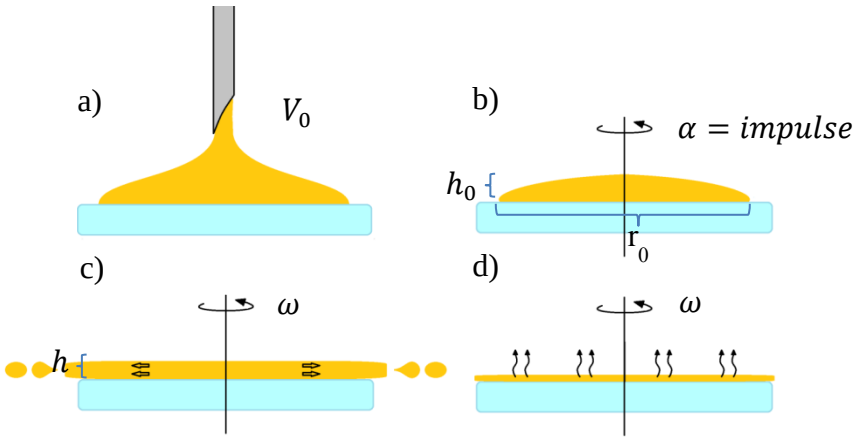

Figure 2.8: Stages of the spin coating process: a) deposition, b) spin up c) spin off d) solvent evaporation

Initial modeling work completed by Emslie et al. [66] gives a relation for the thickness or height, h, of a membrane at the end of a given spin time, t, for stage c) of Figure 2.8.

$$h(t) = \frac{h_0}{\sqrt{\left(\frac{4\rho\omega^2 h_0^2 t}{3\eta_0}\right) + 1}} \tag{2.34}$$

Equation 2.34 relates the polymer the density, ρ, the spin rate, ω, the initial height, h_0, and initial viscosity, η_0, to the height prior to the evaporation stage, for a Newtonian fluid. The initial height can be derived from the volume of a hemisphere, knowing the volume, V_0, of polymer applied to the substrate prior to spinning. The spin up stage is assumed to occur in a very short period of time thus the impulse, α, is neglected from the

calculation. This model does not take into account solvent evaporation (*i.e.* stage d) of Figure 2.8).

The split mechanism model, referring to a two stage process in which the material spinning on the substrate first thins by fluid convection alone then exclusively by mass transfer, was developed by Yonkoski and Soane to account for the evaporation stage [67]. Yonkoski and Soane showed that the transition from stage c) to the stage d) in Figure 2.8 occurs when the rates of film thinning due to each process are equal. The resulting relations for a transition height, h^*, and a transition time, t^*, are shown in Equations 2.35 and 2.36 respectively [67].

$$h^* = \sqrt[1/3]{\frac{3k\eta_0\left[\Phi(w_{s0})w_{s0} - w_{s\infty}^g\right]}{2\rho_p\omega^2}} \tag{2.35}$$

$$t^* = \frac{3\eta}{4\rho\omega^2 h_0^2}\left(\sqrt[3/2]{\frac{2\rho_p\omega^2 h_0^3}{3k\eta_0\left[\Phi(w_{s0})w_{s0} - w_{s\infty}^g\right]}} - 1\right) \tag{2.36}$$

Here, η is the shear-dependent viscosity coefficient, w_{s0} is the initial weight fraction of the solvent in the polymer solution, and $w_{s\infty}^g$ is the weight fraction of the solvent in the gas phase in an infinite atmosphere. The $\Phi(w_{s0})$ term is referred to as a Henry's coefficient and incorporates an exponential correction term on the order of unity defined by Yonkoski and Soane [67]. The mass transfer coefficient, k, takes into account the mass flux of the solvent at the free surface of the membrane and can be estimated at an ambient temperature of 25°C by applying an estimation of the diffusivity of the polymer solvent in air, D_a, the density of air at the ambient temperature, ρ_{air}, and a calculation for the

kinematic viscosity of air, v_a [67]. The equation that relates these values is presented in Equation 2.37.

$$k = CD_a \left(\frac{\rho_{air}}{\rho_{sol}}\right)\left(\frac{\omega}{v_a}\right)^{\frac{1}{2}} \quad 2.37$$

The value of the constant, *C*, depends on the Schmidt number under laminar flow conditions where the Reynolds number is below about 2 x 10^5 [68]. In the laminar flow regime, mass and heat transfer coefficients have been shown to be uniform over the entire rotating disk [68]. Due to this, the Schmidt number is defined by Equation 2.38.

$$Sc_{air} = \frac{v_a}{D_a} \quad 2.38$$

The relation between the *C* and the calculated Schmidt number is presented in Table 2.4 [68].

Table 2.4: Relation between the calculated Schmidt number and C

Schmidt Number	0.74	1.0	2.5	5.0	7.5	10
C	0.33	0.39	0.60	.80	1.0	1.1

The final film thickness, h_f, is determined by assuming that the solvent weight fraction is uniform throughout the film after *t**, this is displayed in Equation 2.39 [67].

$$h_f = h^*(1 - w_{s0}) \quad 2.39$$

2.4.3 Phase Inversion

Most polymeric membranes for industrial use are prepared using the phase inversion process. Simply put, the process involves transforming a polymer in a controlled fashion from the liquid to the solid state [1]. The solidification process is initiated by liquid-liquid demixing where one cohesive liquid state transitions into two. At a certain point, the liquid phase with the higher polymer concentration begins to solidify and a membrane matrix forms. It is possible to define the structure of the resulting membrane matrix by controlling the initial demixing stage [1]. The techniques covered under this process include precipitation by solvent evaporation, precipitation from the vapour phase, precipitation by controlled evaporation, thermal precipitation, and immersion precipitation [1].

The preparation for the phase inversion process usually entails casting the polymer-organic solvent mixture onto a support, which can be porous or nonporous, using a casting knife, dip coating, spin coating, or spraying the support [1]. The following steps are specific to the phase inversion process being implemented but govern the demixing stage. During evaporation, the solvent is allowed to evaporate in an inert (usually nitrogen) atmosphere, to exclude water vapour from the formation process. Control of the rate of evaporation can be achieved by dissolving the polymer in a solvent-nonsolvent mixture. As the solvent is more volatile than the nonsolvent, the solvent will evaporate at a rate proportional to its concentration in the mixture [1]. Alternatively, a vapour atmosphere can be used where the vapour phase consists of a nonsolvent saturated with a solvent. The high concentration of solvent in the atmosphere causes an influx of

nonsolvent into the cast film leading to membrane formation [1]. Thermal precipitation occurs when the temperature is raised or lowered to allow for phase separation and solvent evaporation to occur at a controlled rate [1]. Immersion precipitation acts similarly, whereby the cast polymer solution is immersed in a bath containing a nonsolvent with formation occurring due to the exchange of solvent and nonsolvent [1]. For all phase inversion processes the following factors have a major effect on the resulting structure [1]:

- Choice of polymer;
- Choice of solvent and nonsolvent;
- Composition of casting solution;
- Composition of bath;
- Gelation and crystallisation behaviour of the polymer;
- Temperature of the casting solution and the bath during formation;
- Evaporation time.

Varying any one of these factors can cause changes in polymer structure from open voids to densely packed pores. Membrane properties are determined by the method of production and the manipulation of factors within each method, so the best suited separation process depends on the intended purpose of the membrane.

2.4.4 Membrane Repair

Anisotropic membranes function properly when the selective layer performing the separation, is as thin as possible without pinholes or macrovoids (formed during the

solvent evaporation due to substrate imperfections), and without the presence of dust particles [19]. The gas flux is inversely proportional to the thickness of this separating layer. However, as the membrane thickness decreases, the probability of forming pinholes increases. These imperfections are difficult to eliminate and, although they may not significantly affect the performance of anisotropic membranes used in liquid separations, they can render the membrane useless in GS processes [19].

To address this, various polymer specific methods of casting or post-treating have been developed [69]. Unfortunately, most of these methods increase the density of the surface layer in contact with the feed stream, which reduces the overall gas flux of the membrane [69]. High flux membranes can be prepared after the selective layer has been repaired using a relatively non-selective, highly permeable "caulking" layer. Conceptually, the implications for membrane flux can be related to Ohm's law which describes current flow through a resistor (Equation 2.40).

$$I = E/R_x \tag{2.40}$$

Current, I, electric potential, E, and electrical resistance, R_n, are analogous with permeation rate, concentration (or partial pressure) gradient, and resistance to permeant flow, respectively [69]. Composite membranes consisting of a selective membrane coated or "caulked" with the non-selective membrane is analogous to a series-parallel array of resistors (see Figure 2.9) [18].

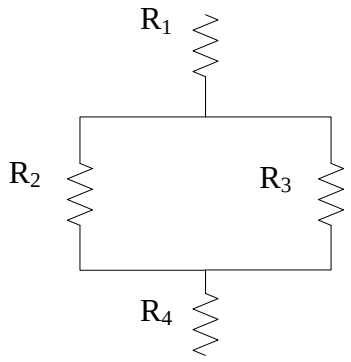

Figure 2.9: Series-parallel array of resistors representing the resistance to flow with an additional non-selective layer

In the ideal case, the "caulking" material will only fill the existing porous defects on the surface layer of the membrane. However, in practice, a small amount will coat the non-defective regions as well [17]. The intrinsic membrane resistance to flow for component i of this system can be calculated as the sum of two resistors in series and an equivalent resistance according to Equation 2.41 [18].

$$(R_{in})_i = (R_1)_i + \frac{(R_2)_i (R_3)_i}{(R_2)_i + (R_3)_i} + (R_4)_i \qquad 2.41$$

The resistance R_1 is the "caulking" layer, R_2 and R_3 are the dense surface layer and the pinholes or macrovoids, respectively, and R_4 is the bulk separating layer [18]. Ideally, R_4 will have a negligible resistance in comparison to the other resistances and R_3 will have increased 10^5 to 10^6 fold. This occurs for even the most permeable polymers after the pores have been filled by the "caulking" material, when compared to an open pore of similar depth [69]. The expression for the resistance of the pores can be represented using the intrinsic permeability of the gas in the specific layer being analysed, $P_{i,x}$, and the thickness of that layer, l_x (Equation 2.42) [18].

$$(R_x)_i = \frac{l_x}{P_{i,x}} \quad 2.42$$

By combining Equation 2.26 and 2.31, from Sections 2.2.1 and 2.2.2 respectively, it can be shown that Equation 2.42 is the inverse of permeance. As noted earlier, the resistance of the pinholes, R_3, increases dramatically due to caulking such that the second term in Equation 2.41 becomes approximately equal to R_2. By substituting Equation 2.42 into Equation 2.41, a relation between overall permeance and the total layer resistance can be formed (Equation 2.43).

$$Q_i = \frac{J_i}{\Delta p_i} = [(R_1)_i + (R_2)_i]^{-1} = \left[\frac{l_1}{P_{i,1}} + \frac{l_2}{P_{i,2}}\right]^{-1} \quad 2.43$$

This confirms that to optimize a "caulked" membrane, the added material must have a high permeability for the specific gas and be applied as thin as possible to reduce the added resistance to flow. External resistive factors such as membrane fouling (outlined in Section 2.1.3.1) can be easily combined with Equation 2.43 as resistive values in series and would be specific to the substances used in the feed stream.

2.5 Membranes for Sensor Applications

There are three groups of properties to be considered when selecting an appropriate membrane for a given sensing application. These are: the transport behaviour of the polymer (*i.e.* permeability, selectivity, and transmembrane potential); how well the membrane acts as an immobilization matrix, and; properties relating to surface/interface behaviour [70]. Sensing applications requiring robust membranes must have properties ranking high in all of these categories: *i.e.* absence of microdefects affecting the

transport behaviour; high thermal and chemical stability (appropriate for the given application) preserving the separation characteristics; a relatively low reduction in permeability and permselection due to aging and; good mechanical stability [54].

The transport properties of a membrane are the most important of these properties. For a sensor/membrane system to effectively detect a given permeant, the membrane must filter and transport that permeant across the membrane in a reasonable time to be detected. For biosensors specifically, permeant detection involves either the immobilization of a substance sensitive to a change in target permeant concentration (*i.e.* pH or fluorescence-based sensors) or it can involve direct detection of permeant specific properties (*i.e.* a change in the physiochemical properties of the sensing environment). Membranes are employed to separate the sensing environment from contaminants, rejecting the majority of confounding species and particulates. However, the rate determining step for most membrane/sensor systems is the rate of diffusion of the target permeant across the membrane [70]. This limits the response time of the sensor and can allow for interfering ions to affect the signal.

2.5.1 Carbon Dioxide Sensors

In many CO_2 sensors, a gas separating membrane is used to isolate CO_2 for detection. The first dissolved CO_2 detection system was built by Richard Stow in 1954 and later improved upon by Dr. John W. Severinghaus for the purposes of blood gas analysis [71]. The initial pH-based CO_2 sensing device used silicone rubber, and later switched to Teflon, to separate CO_2 from blood to a bicarbonate buffered solution for a pH measurement [71], [72].

Most commercially available dissolved CO_2 sensors use the Severinghaus principle to facilitate sensing. However, a number of disadvantages of this basic sensor exist including a high cost and the potential for electrical and chemical interference. More recently, sensors with alternative membrane transport characteristics or combinations of multiple types of polymer membranes have been investigated to improve sensor response time and accuracy. Xie and Bakker report a potentiometric based sensor, implementing a carbonate selective membrane, to detect variations in pH caused by the presence of carbonate. Schutting and Borisov implemented a thin fluorescent sensing film covered with a gas-permeable silicone layer to detect gaseous CO_2 in the 100's of ppm range [73], [74].

An important stream of CO_2 sensor for remote environmental monitoring incorporates the use of fiber optics. The ability of these so called 'carbon dioxide optodes' to transmit long distances with very low losses, their innate immunity to electromagnetic interference, and their ability to function far removed from any electrical components makes these sensors ideal for many types remote sensing. A number of sensing modalities have been presented that exploit various well known properties of CO_2, such as the refractive index (RI), the pH of a CO_2 solution, and polymer adsorption of CO_2 gas. These properties have been used for sensing both on their own and in various combinations.

While direct measurement of the RI of CO_2 gas has not been widely reported, as the difference in RIs is sufficiently small at atmospheric conditions, Bao et al. has presented a sensor that can distinguish the difference in RI between supercritical CO_2 and

a CO_2 saturated brine solution as well as the difference between brine and a similar solution [75]. This sensor uses the light scattering properties of a long period fiber grating (LPFG) in which light traveling within the core of an optical fiber couples out to the cladding modes and is able to interact with the surrounding media.

Optical pH sensors for the detection of CO_2 in solution generally use one of two types of configurations, transmission mode or reflection mode, and are based on either absorption or fluorescence methods [76]. Sensors based on the absorption method are generally more difficult to miniaturize, especially in transmission mode and are usually not selected when the fluorescence method is an option [76]. Sensors based on the fluorescence method use a pH indicator dye that is immobilized on either the tip of a fiber (eg: [77], [78]) or in line with the fiber (eg: [79]). The fiber in the reflection mode configuration is dead ended in the target solution and a measurement of fluorescence intensity is made that can correlate with CO_2 concentration, the sensitivity of which depends on the pH operating range of the dye used. To modify the light traveling in the core of the fiber in response to the presence of CO_2 for the transmission mode configuration, the 'in-line sensor' requires that the pH sensitive dye be immobilised close to the core of the fiber. These sensors do however, suffer from instabilities in sensitivities due to leaching of the pH indicator and microbial fouling in long term deployments [80].

The above mentioned sensing methods are not inherently selective and without the addition of a membrane to separate confounding substances, compounds that alter the sensing environment's pH, RI, or fluorescence can cause a misreading of the presence of CO_2. In isolated bench top conditions, as many of the proof of concepts are

accomplished, these sensors may give high sensitivities to changes in CO_2 concentrations but without specificity, they will not be accurate enough for implementation in the field.

2.6 Summary

The application of a dense polymeric membrane to separate gases for sensing purposes requires the understanding of the trade-off between permeability and permselectivity. This relationship, for many gas pairs and polymers, has been well mapped by Robeson. The cluster of polymers investigated for CO_2/N_2 separations based on lab scale, controlled experiments, is displayed in Figure 2.4. The empirical upper bound discovered by Robeson is a good guide to evaluate polymer performance in a comparative manner, however many more membrane attributes effect the performance in a given application. Pin holes, or MVs, can form during membrane casting allowing permeants to bypass the separation qualities of the membrane. Fouling and aging of a membrane can occur after continual use and can alter the intrinsic properties of the membrane as well (*i.e.* diffusion and solubility characteristics).

The formation process of a membrane and final filtration configuration can also alter the final separation properties. This includes: the organic solvent used to create the polymer solution; the method of forming the final membrane; the membrane geometry; the membrane configuration and; the nature of the polymer back bone. The membrane's mechanical stability, tolerance to feed stream components, tolerance to potential temperature variations and ease and cost of manufacturing must also be considered. The target application's environment in terms of the pressure, temperature, and local

substances present (*i.e.* particulate, gaseous, or aqueous) should also be taken into consideration when selecting potential polymer candidates for membrane formation.

In the event of membrane formation defects, repairs can be made to membranes that have MVs using a relatively non-selective caulking membrane layer. The filler membrane causes a high resistance to flow in MVs formed during the formation process due to the small volume that the polymer fills. Since the caulking membrane is not selective, the thin layer on the surface of the selective layer should not impede gas flow significantly to the underlying selective layer.

Membranes provide the selectivity necessary to detect substances using methods that are inherently not selective (*i.e.* RI, pH, and fluorescence). It may be possible to show that the sensors used to detect substances, like CO_2, have a high sensitivity when exposed to the analyte exclusively in controlled conditions. However, when these sensors are exposed to substances that may be able to alter the sensing environment they will not be able to separate responses due to confounding substances.

Chapter 3: Experimental Methods

3.1 Commercial Polymer Selection

Commercially available PBI S10 and VTEC PI 1388 were selected for investigation in this study. Characteristics of each polymer are presented in this section.

3.1.1 PBI S10

The PBI S10 solution, provided by PBI Performance Products Inc., was selected due to its robust nature, high glass transition temperature, resistance to solvents once cast, and attractive CO_2 permeability. Attempts were made to create a PBI solution for comparison purposes using solid pellets of PBI however, as the solid PBI is only soluble after heating to high temperatures for long durations in highly polar, aprotic organic solvents, such as dimethyl sulfoxide (DMSO), N,N-dimethylforamide (DMF), DMAc, and NMP, and the process yield is not easily measured, this work was abandoned [15], [63]. The physical properties of the S10 solution were provided by PBI Performance Products Inc. and are displayed in Table 3.1.

Table 3.1: Properties of PBI S10 solution

Property	Value
Solids [%w/w]	9±0.5
Solvent (DMAc) [%w/w]	91
Viscosity [cP]	90±20

3.1.2 VTEC PI 1388

Due to its use in similar analyses involving gas separating membranes and because its development was based on the results of the PBI testing, the VTEC PI series

was also explored [15]. Specifically, the VTEC PI 1388 polymer from R. Blane Industries was acquired, as it had been reported to have higher gas permeabilities and selectivities for the gases being analysed in this report when compared to PBI and relatively similar transport properties when compared to the other VTEC polymers.

3.2 Membrane Formation

Asymmetric membranes were formed using a modified phase inversion method. The simplest phase inversion method is knife casting of polymer solutions on to an appropriate substrate followed by solvent evaporation in an inert atmosphere, to exclude water vapour [1]. This method was not selected however due to the inherent difficulty in creating a forming rig that would consistently yield uniform ultra-thin membranes with micron accuracy. Instead, a spin coating process was employed in an effort to create similar results to a higher degree of accuracy.

The solvent evaporation stage of the phase inversion process begins during the spin coating process, after the spin off stage was complete. To remove any remaining solvent or water vapour to complete the phase inversion process, the semi-cast polymers were placed in an oven at temperatures specific to that polymer. The VTEC and PBI polymers were provided pre-dissolved in solvent at 20±1.0% and 9±0.5% weight percent solids respectively. The Rohm and Haas high molecular weight PVC powder, 100-200 mesh, was mixed to a 40% w/w DOP/PVC in THF at 3±2% w/w PVC/THF separately.

3.2.1 Spin Coating and Heat Treatment

Prior to being applied to the glass substrate, the polymers were allowed to equilibrate with the ambient room temperature as suggested by the manufacturer. This was accomplished by extracting 10 mL from the bulk polymer container with a syringe and leaving it out for approximately 30 min prior to application. Using a G3B-8 spin coater, manufactured by Specialty Coating Systems, a target spin rate, acceleration time, and spin duration were selected. The cumulative spin time was set to either 30 or 45 sec, depending on the trial, and the acceleration time to the target spin rate was set to a constant 3 sec for all trials.

Polymer solution was placed on a 3/4” diameter glass disc substrate, forming a hemi-spherical dome on the surface of the substrate prior to spinning. The volume applied was trial dependant. The spin rates dictated the final membrane thickness and the range of selected rates were largely based on the respective polymer viscosity. The range of spin rates investigated for the DOP/PVC, VTEC PI 1388, and PBI were 500 to 1200 rpm, 2000 to 4000 rpm, and 600 to 1000 rpm respectively. The limits on the rates were set empirically, as on the lower end of the spectrum the membranes were generally too thick to allow for subsequent flux experiments and on the higher end were unable to be removed from the glass substrate without tearing, creating voids, or compromising structural integrity and filtering ability.

Most membranes can be formed through thermally-induced phase inversion processes [17]. The process used in the formation of the membranes used in this research was precipitation by solvent evaporation. Each membrane was placed within an oven, set

to a temperature slightly above the boiling point of the solvent in the polymer-solvent solution, and allowed to cure. The polymer specific settings for both the spin coat process and heat treatment processes are provided in the following sections.

3.2.1.1 VTEC PI 1388

The relationships between spin rate, spin time, the amount of polymer applied to the substrate, and the final membrane thickness were investigated using the VTEC PI 1388. Three sets of trials were completed to determine a relationship between the three variables and their effect on the final thickness of the membrane after curing.

Initially, 0.2 mL was applied to the substrate. This was the minimum amount in which the glass substrate was fully wetted prior to spinning. Spin rates from 2000 to 4000 rpm were investigated at intervals of 100 rpm to determine the thinnest possible membrane that could reliably be removed from the substrate without membrane failure at a total cumulative spin time of 30 sec. Following this, the spin time was increased to 45 sec, holding the amount applied to the substrate constant. A reduced window of spin rates was investigated, from 3000 to 3500 rpm, as outside of this interval the membranes were not forming reliably. Finally, holding the spin time at 45 sec, the amount applied to the substrate was increased to 0.6 mL. This was the largest amount of VTEC PI 1388 that could be applied to the substrate without over flow. Spin rates from 2500 to 4000 rpm were investigated at intervals of 100 rpm.

For final membrane formation, a 10 μm membrane thickness was targeted which corresponded to spin rates between 3000 and 3300 rpm and a spin time of 45 sec for 0.6

mL of applied solution. To cast the membrane, the spin coated glass substrate was placed in an oven at 130°C for 30 min followed by 200°C for 20 min.

3.2.1.2 PBI

In a similar procedure aimed at reducing the frequency of membrane imperfections, the optimal spin rate and applied volume was determined for the PBI. Since the polymer solution was much less viscous when compared to the VTEC, much lower spin rates were implemented. The first sets of membranes were fabricated using 0.2 mL of solution at spin rates from 500 to 1000 rpm. Following this, the spin time was increased to 45 sec and the spin rate narrowed to 600 to 900 rpm. Finally, the applied volume was increased to 0.4 mL holding the range of spin rates and spin time constant.

Again, a 10 μm membrane thickness was targeted for final membrane formation. This corresponded to spin rates between 600 and 800 rpm and a spin time of 45 sec for 0.4 mL of applied solution. To cast the membrane, the spin coated glass substrate was placed in an oven at 110°C for 30 min followed by 180°C for 20 min.

3.2.1.3 DOP/PVC Mixture for Caulking Layer

Once it was determined that forming an ultra-thin membrane either out of PBI or VTEC PI without pinholes present would be unlikely under normal fabrication conditions, the method of sealing or "caulking" the membranes was adopted [81]. This method involved creating an entire caulking layer on top of the selective membrane layer and was employed to seal very small membrane defects. By fully coating the selective membrane layer, it was insured that all of the MVs were sealed as many of these

imperfections were not able to be detected under optical magnification. Readily available PVC was chosen and mixed with the DOP plasticizer to create a rubbery, relatively non-selective, highly permeable, hydrophobic membrane. THF was used as the organic solvent to dissolve the PVC and DOP. The mixture ratios that were created to investigate the impact of the spin rate and the DOP w/w% on the final membrane stability were approximately 20 to 80% DOP by weight. Measurement of liquid solvent and plasticizer was accomplished using a micropipette with a random error max of 0.68% and measurement of powdered PVC was accomplished using a digital scale with accuracy to ±0.001g. Mixture ratios are presented in Table 3.2.

Table 3.2: Ratios of components in the investigated non-selective hydrophobic "caulking" solutions

Batch	PVC/THF	DOP/PVC
1	5.4%	20.0%
2	5.5%	31.0%
3	5.8%	40.0%
4	5.2%	50.0%
5	5.2%	60.8%
6	5.3%	70.3%
7	5.4%	79.8%

The optimum mixture of DOP/PVC was determined empirically. Qualitatively, it was observed that once the polymers were cast, and removal from the glass substrate was attempted, the 20% mixture was too glassy and cracked and the 60% mixture was not cohesive enough to maintain self-support. The 40 w/w% DOP/PVC was selected for continued investigation as the mixture formed rubbery-like membranes that were able to

be cast sufficiently thin and maintain their structural stability. Larger quantities of the 40% mixture were created to facilitate a larger sample size.

With a target of >10 μm for the non-selective DOP/PVC caulking layer, spin rates between 500 and 700 rpm were investigated, with a spin time of 45 sec and 0.4 mL solution applied to the glass substrate. The caulking layer was spun over the pre-cast selective membrane layer and subsequently cast in an oven at 50°C for 30 min.

3.2.2 Thickness Measurement Techniques

The membranes were divided into four quadrants for measurement and an average of all four measurements was taken. Measurements were collected using a Mitutoyo Digimatic Micrometer, to an accuracy of ±2 μm, in the order displayed in Figure 3.1. When multiple membranes were cast subsequently on to the same substrate, a differential measurement technique was employed. An inverted 'T' was placed on the side of the glass substrate to mark the location of the first quadrant as well as the non-coated side of the substrate. Each subsequent thickness measurement was taken moving counter clockwise from the initial quadrant. The average quadrant thickness of the glass substrate, the selective membrane layer, and the caulking layer were recorded (M1, M2, and M3 respectively in Figure 3.1).

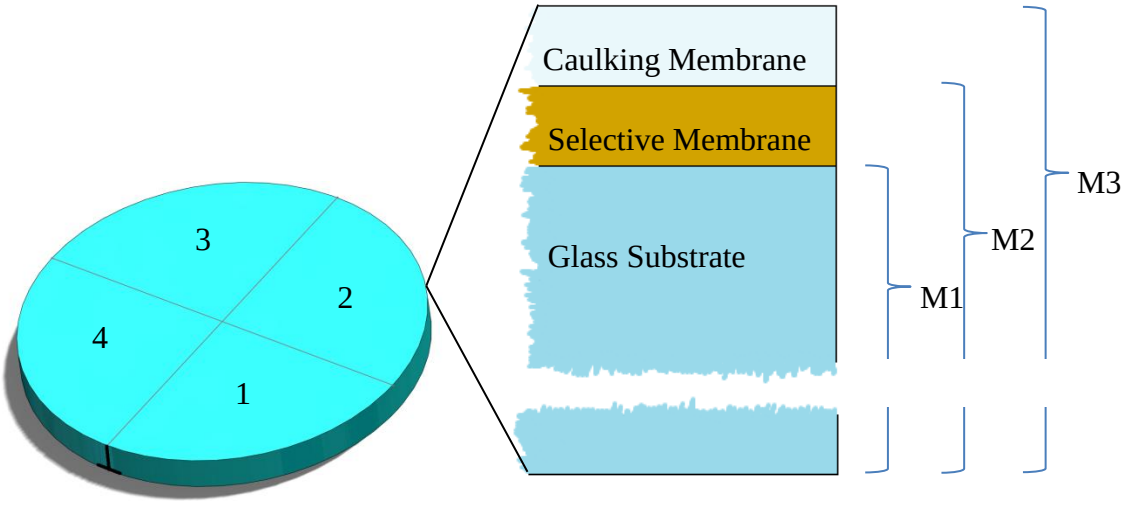

Figure 3.1: Quadrant measurement numbering and multi-membrane measurement method

To determine the thickness of the selective membrane, the difference between the average quadrant thicknesses measured at M2 and M1 was calculated and for the caulking membrane, the difference between the average quadrant thicknesses measured at M3 and M2 was calculated.

3.2.3 Removing the Cast Polymer from the Substrate

Using a Meiji EMZ-TR optical microscope and accompanying Meiji fiber optic light source (FL 180), a small portion of the edge of the cast polymer was lifted from the glass substrate around the entire circumference of the disc. This formed an air bubble between the glass substrate and the membrane. This was accomplished using a no. 10 pointed tip X-Acto knife.

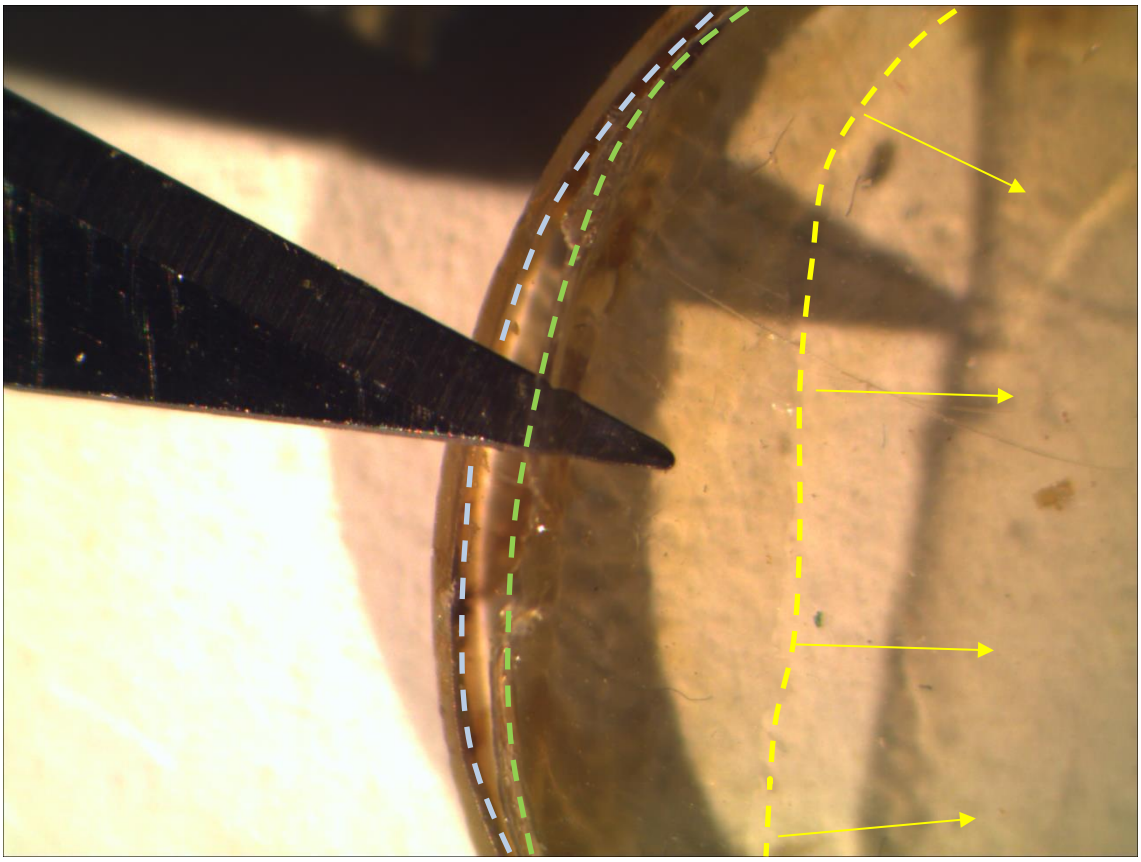

Figure 3.2: Mechanically lifting the membrane edge (green line) from the glass substrate (blue line) to allow air bubble propagation (yellow line) and subsequent membrane removal

Once the edge was freed, the point of the blade was slowly moved under the polymer, forming an air bubble. This bubble was slowly spread under the polymer using the blade in the direction of least resistance carefully around the circumference of the disc. Once the bubble was worked around enough to expose at least half of the underside of the cast polymer, the remaining amount could be peeled back by hand. So that less patching would be required, care was taken not to allow larger holes to cause tears in the membrane during removal.

3.3 Repairing Macrovoids

To repair visible macrovoids (MVs), as shown in Figure 3.3, that have formed throughout the membrane, a non-permeable resin was used. Each MV was located by eye using a Meiji EMZ-TR optical microscope and accompanying Meiji fiber optic light source.

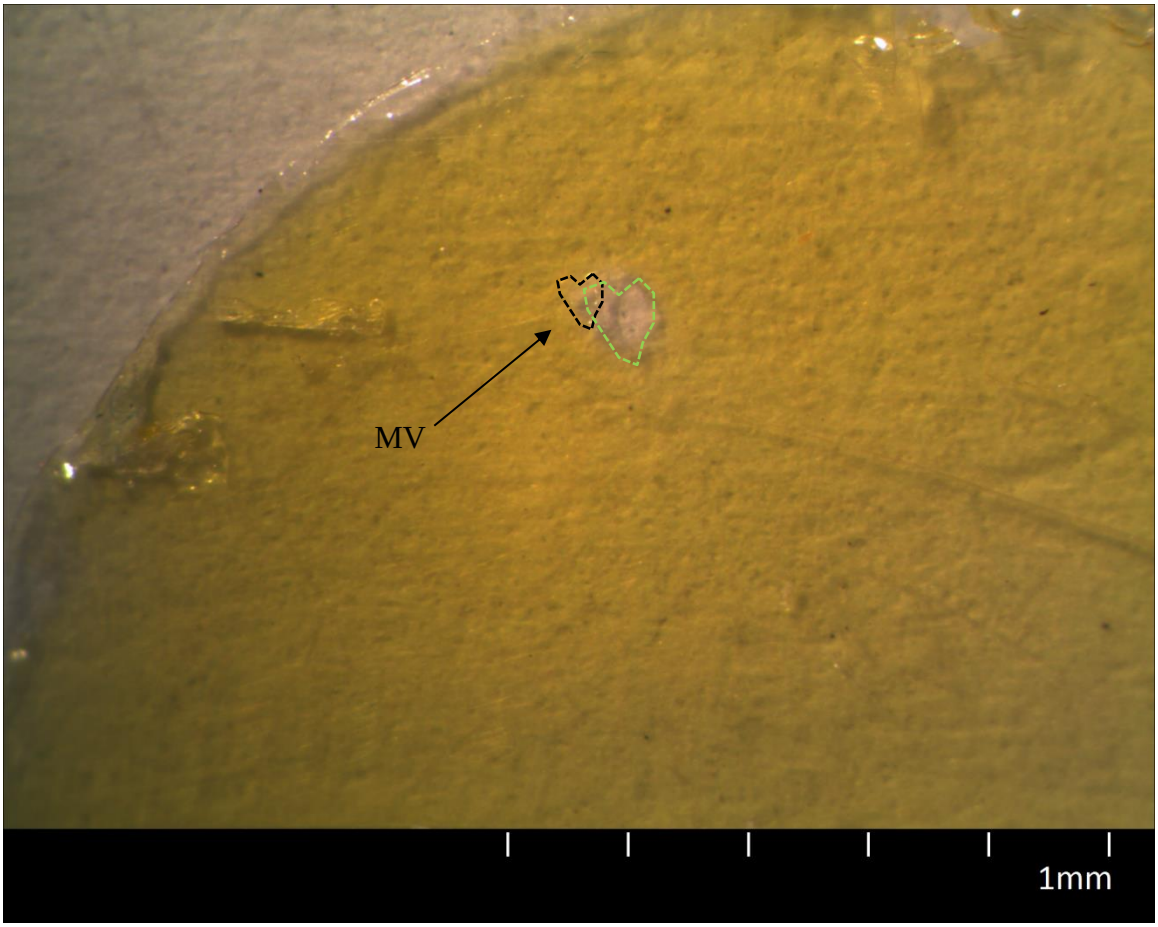

Figure 3.3: ~200 µm macrovoid (black dotted outline) formed in VTEC 1388. MV outlined allows unfiltered light to pass through the membrane causing the surface below to be seen differently to the right due to angle of scope light (green dotted outline)

Generally, these MVs occur during casting and are at least 10-50µm in diameter [82]. Once located, the larger MVs were sealed with a patch of solid VTEC PI 1388 or

PBI applied over the void. Following this, the patches were sealed in place using the resin to close the void. For small enough MVs, the material patch was unnecessary and resin was used exclusively as a sealant. The resin was applied to the intended feed side of the membrane and was accomplished using a very fine paint brush. For the multi-layer membranes, the patching resin was applied both on top of the caulking layer as well as on the underside of the membrane. The patching locations are displayed in Figure 3.4.

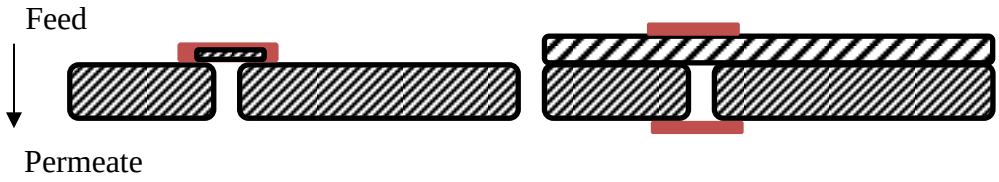

Figure 3.4: Single separation layer resin patch (left) and multi-layer resin patch (right)

Since the membranes are very thin, these voids opened the separation membrane from surface to surface and allow throughput of gas particles without filtration. Patching resin was, therefore, applied generously around the MV to insure sealing as depicted in Figure 3.5.

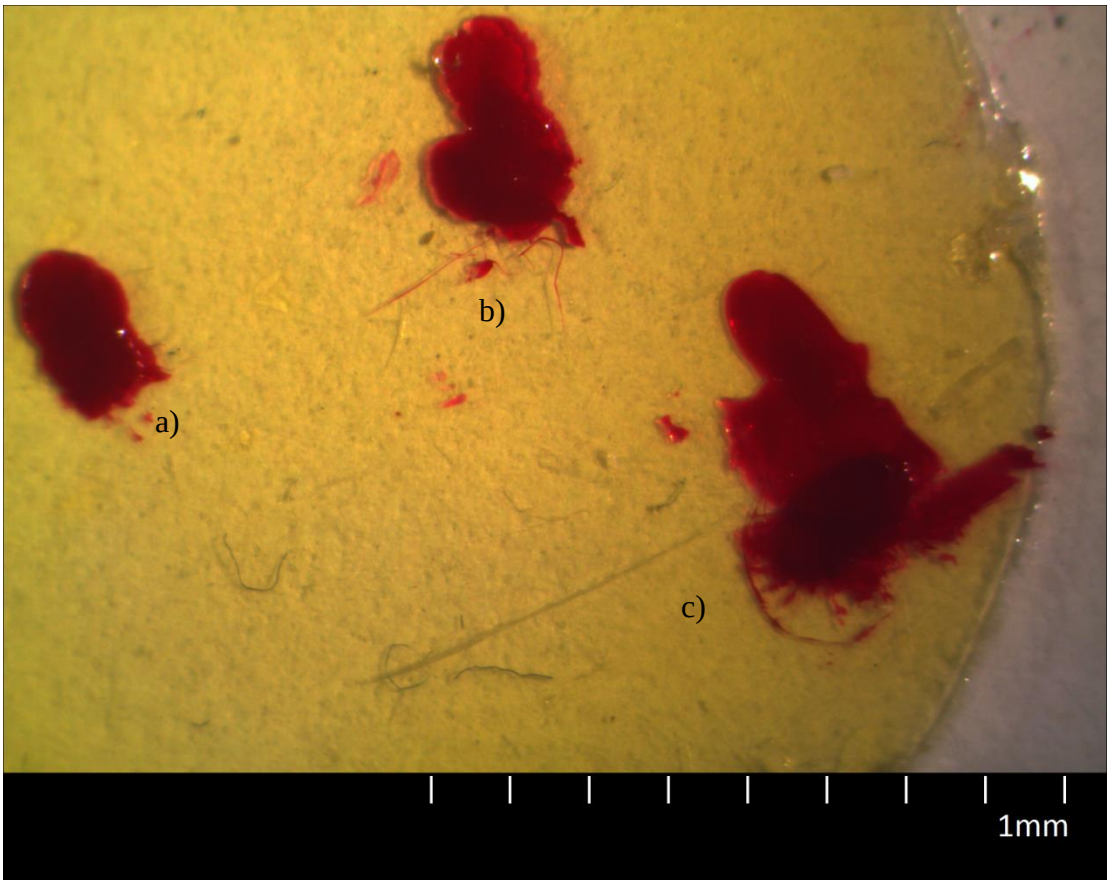

Figure 3.5: Patched VTEC1388 membrane with patch areas of a) 3.99mm^2 b) 2.78mm^2 and c) 8.93mm^2

Although the MVs in Figure 3.5 were 10 to 100 µm in diameter, the patches were applied with diameters >1 mm. All reductions to gas fluxes incurred by these patches were taken into account when permeabilities were calculated.

3.4 Volumetric Gas Flow Characterization

Methods for measuring the gas flux characteristics under temperature and pressure controlled conditions are presented in this section. Test setup specifications and control conditions are outlined along with the specific measurement equipment used.

3.4.1 Set-up

Each membrane, after being caulked and repaired, was placed within the membrane testing unit (MTU) displayed in Figure 3.6.

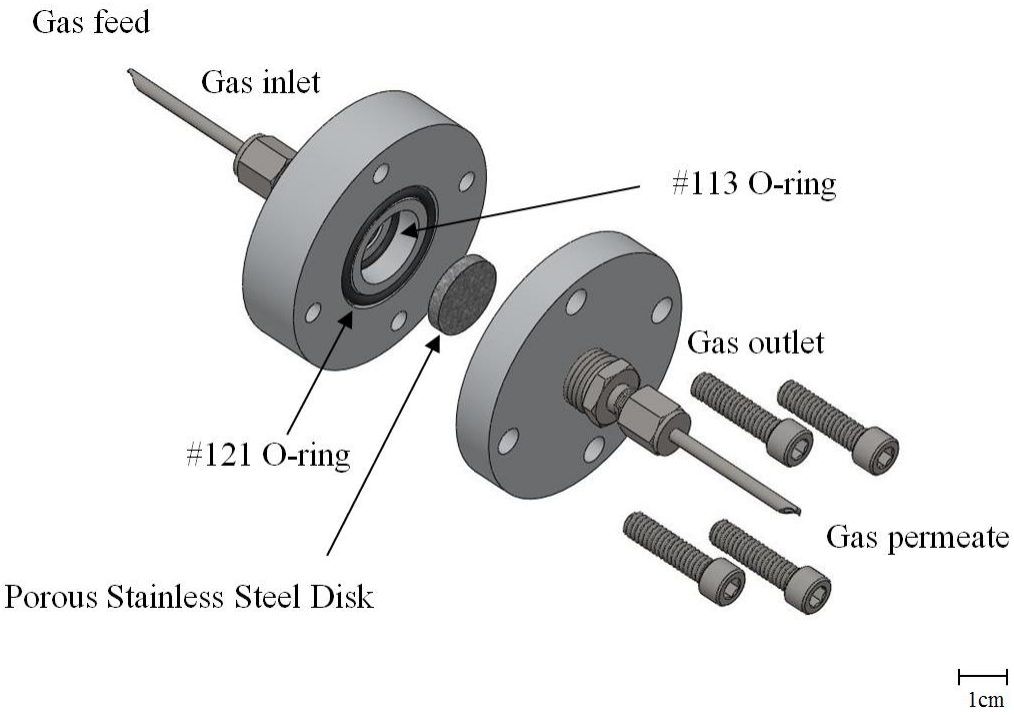

Figure 3.6: Membrane Testing Unit (MTU) Assembly

The main body of the MTU was created from two stainless steel cylinders with a diameter of 2.5" to accommodate the centralized porous metal disc, O-rings, and securing screws. A #121 O-ring was used to create a seal between the gas feed and gas permeate streams. The membrane was placed directly on a 10 μm porous stainless steel disc, 1/16" in thickness, 3/4" in diameter, on the feed stream of the MTU. A #113 O-ring was placed in between the internal gas inlet and the membrane and another on the permeate side of the porous stainless steel disc to prevent gas flow around the membrane. The MTU was

sealed using 4 fully threaded stainless steel socket head cap screws (1/4”-20) and attached to 1/8” stainless steel tubing at both the inlet and outlet such that the membrane was in the dead-end configuration (Figure 3.7).

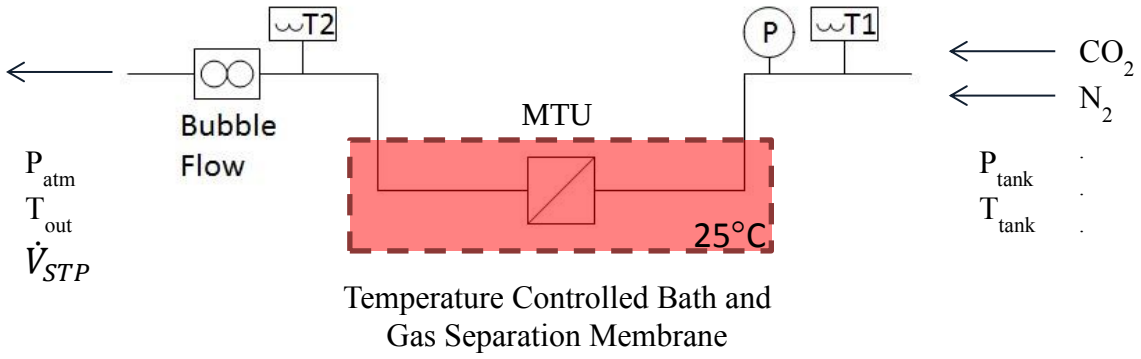

Figure 3.7: Flow schematic for the gas characterization set-up

An analog pressure gauge (Swagelok 0-300 psi) at the gas inlet (not shown), pressure transducer (Omega PX309-150G5V), P, and resistance temperature detectors (Omega RTD-NPT-72-E), T1 and T2, were built upstream of the membrane for online pressure and temperature monitoring of the feed stream using T-junctions. Another RTD monitored the permeant as it flowed out through a bubble flow meter (10 mL Sigma-Aldrich), which was open to the ambient temperature and pressure. The accuracy of the transducer was 0.25% FS or ±0.75 psi and the accuracy of the RTDs (Class “A”) were 0.2°C at 25°C. The majority of the 1/8” stainless steel pipe and the MTU were submerged in a 12 L temperature controlled bath (Thermoscientific) at 25°C. Pressure on the downstream side of the MTU was taken as the local barometric pressure measured at a

weather station on the University of Victoria science building provided by the School-Based Weather Station Network. The data recorded by this station is up to the minute real time data (www.victoriaweather.ca).

3.4.2 Membrane Characterization

For the membrane to have a basis for comparison to other published data, the gas diffusion characteristics of the separation membrane needed to be determined. For this purpose, two industrial grade gases CO_2 and N_2 (Praxair) were attached to the feed side of the membrane for their respective trials. The gas was held at set pressures of 20, 30, 40, 50, and 60 psi while the volumetric flow was measured. For each set pressure, the measurement was repeated a total of three times. Online recording of temperature and pressure occurred throughout all trials for a given gas using a LabView application. Volumetric flow was measured using a bubble flow meter (Sigma-Aldrich), by eye, in which the time it took a bubble to flow 1 mL was recorded. This provided a flow rate in mL/sec and was used in subsequent flux calculations compiled using MatLab.

3.4.3 Analysis

After removing the membrane from the MTU, the filtering surface area was measured. The filtering surface area is depicted in Figure 3.8 and is a measurement of the area not blocked by the compressed O-ring after securing within the MTU was recorded.

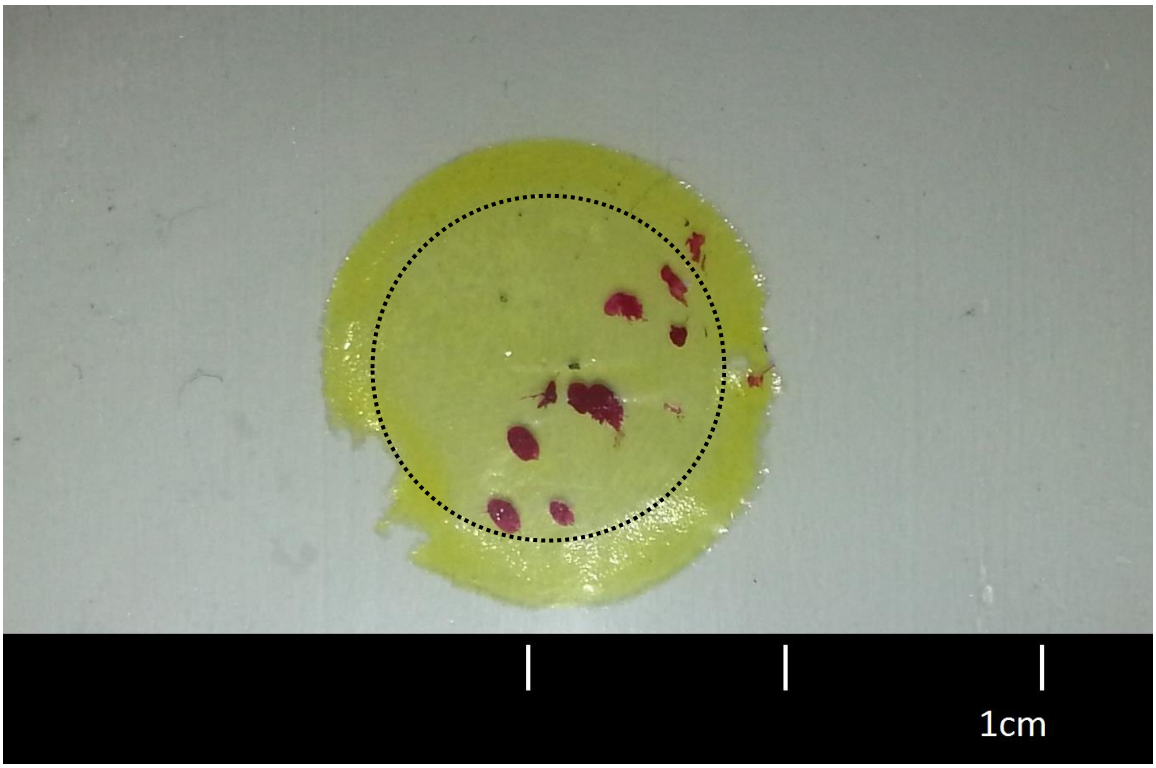

Figure 3.8: Dotted area indicating the outer boundary of the filtering surface area after O-ring compression. The cumulative area of the eight patches contained within the filtering surface area is subtracted to yield the reduced filtering surface area.

Accurate measurement was accomplished using software package imageJ. Both the filtering surface area and each of the patched MV's were measured 3 times and each set of measurements was averaged. The sum of the average surface areas of the patched MV's was subtracted from the filtering surface area and the reduced filtering surface area was used with equations 2.32-2.33 to calculate flux, permeability, and permselectivity respectively.

Chapter 4: Results and Discussion

4.1 Membrane Formation Results

The majority of the membranes formed using the modified phase inversion method outlined in Section 3.2 had multiple MVs causing uncharacteristically high volumetric flow rates. This was experienced in the PVC caulked and un-caulked VTEC PI 1388 as well as the PBI membranes. Spin coating settings that caused membranes to either form too thick to allow for a measurable flow to occur or too thin causing tears at higher pressures were also an issue. A decision was taken to concentrate only on the VTEC PI 1388 membranes in an attempt to decrease the time required to develop an improved process. A target membrane thickness of 10 μm was determined for the spin coating process. At this thickness, repeatable intact membranes without MVs were able to be created. After optimizing the methods used to form the VTEC PI 1388 membranes, PBI membranes were then created using the successful methods.

4.1.1 VTEC PI 1388 Processing and Initial Gas Flow Results

Figure 4.1 displays the effect of the spin coating settings on the final thicknesses of the VTEC PI 1388 membranes.

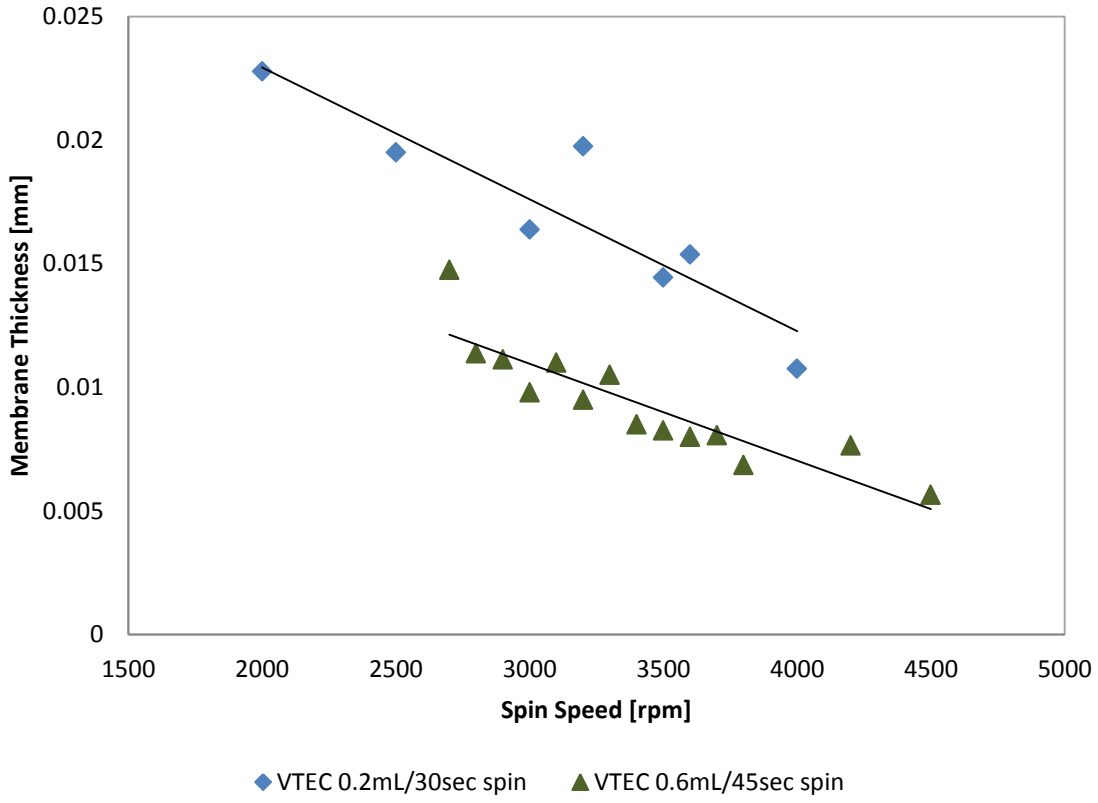

Figure 4.1: Effect of spin rate, spin time, and volume of polymer applied on average final VTEC PI 1388 membrane thickness

Initial measurements were taken of each successful membrane produced resulting in negative linear correlations between membrane thickness and the spin speed of the spin coater for each data set. With a target of 10 µm, 0.2 mL of polymer was deposited on the glass substrate and spun for 30 seconds. The resulting membranes were unable to form successfully below ~15 µm repeatedly. Since there was a smaller mass acted upon by the centrifugal forces, more material remained on the surface initially forming thicker membranes. With less time to form the membrane layer, more MVs, non-uniform coatings of the glass substrate, and less structurally sound membranes were created. By

increasing both the volume applied to the glass substrate and the spin duration, it was expected that more uniform membranes would result. The 0.6 mL polymer volume, spun for 45 sec, resulted in thinner membranes that were able to be spun at higher rates without loss in integrity. The difference in trend between the two data sets indicates that the larger volume of polymer applied was in excess of the amount required form membranes at the rates investigated. The material spin-off for the larger volume of applied polymer occurred in a shorter period of time when compared to the smaller volume trials. This allowed for more uniform solvent evaporation and polymer thinning without MVs forming as well as making the 10 μm membrane thicknesses achievable with a higher success rate.

The initial data collected yielded high volumetric gas flow rates (for both CO_2 and N_2) this was associated with the presence of an MV as the volume of polymer applied prior to spin coating was varied and the membrane was caulked. This resulted in a secondary method for detection of MVs that were not located and sealed during the initial visual inspection prior to mounting in the MTU. The high volumetric gas flow rates are displayed in Figure 4.2.

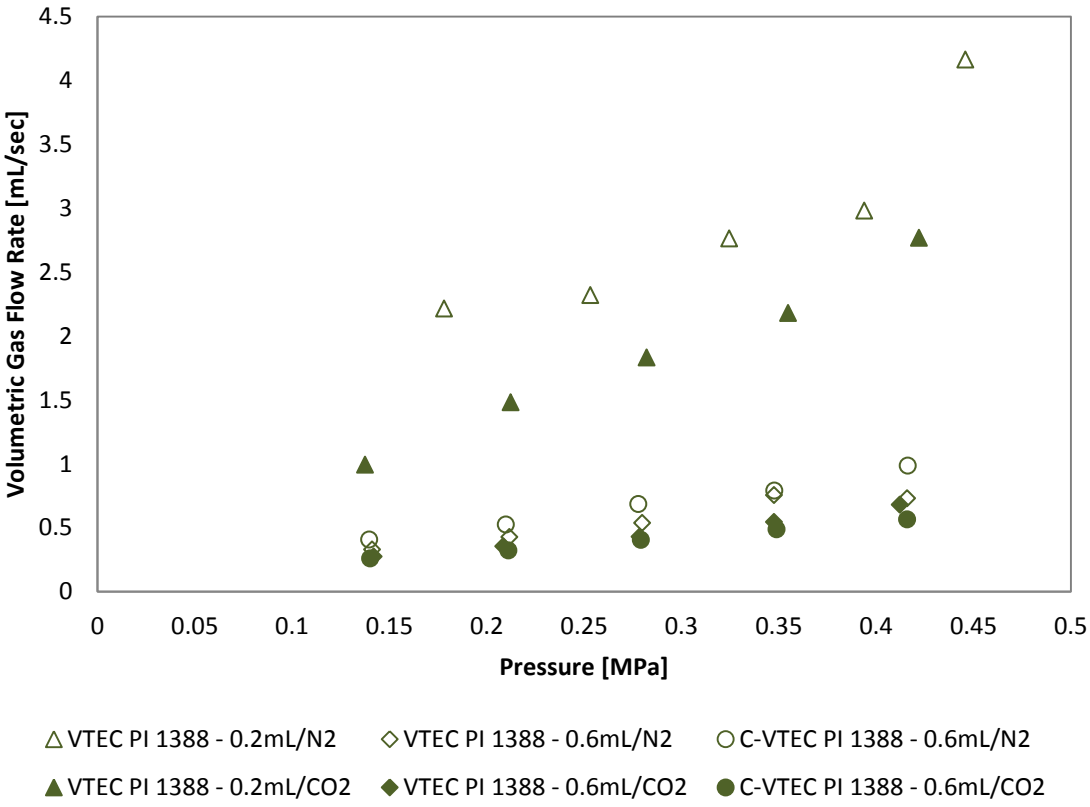

Figure 4.2: Average VTEC PI 1388 volumetric gas flow rates (using CO_2 and N_2) indicative of MVs for caulked and un-caulked VTEC PI 1388 (c-VTEC PI 1388 and VTEC PI 1388 respectively)

A major factor affecting the gas flow rate is the membrane thicknesses investigated which are largely influenced by the spin rates applied prior to heat treatment. The thicknesses of the membranes selected for testing for the 0.2 mL applied volume were an average of approximately 19 μm spun at 2900 ± 590 rpm. These membranes had the largest concentration of MVs and due to this produced the highest volumetric flow rates even though, on average, they were the thickest. The thicknesses of the membranes selected for testing for the 0.6 mL applied volume were an average of approximately 7

μm and were spun at 3600 ± 94 rpm. By increasing the amount of VTEC PI 1388 applied to the glass substrate prior to spin coating, the point-by-point percent change in volumetric flow rate, comparing the membranes formed using a smaller volume of applied polymer to those formed using a larger volume, was overall an 81% and 75% decrease for N_2 and CO_2 respectively. This indicates a substantial decrease in the concentration of MVs and shows an improvement in overall membrane processing procedures. Faster spin rates were able to be achieved that produced thinner membranes. After caulking the membranes the point-by-point percent change in volumetric flow rate, comparing the un-caulked to caulked membranes, incurred another decrease of approximately 23% and 10% for N_2 and CO_2 respectively. The VTEC PI 1388 portion of the caulked membranes averaged approximately 4 μm in thickness having been spun at 3600 ± 600 rpm. Even though a reduction in overall volumetric gas flow rate was realized, the corresponding permeabilities to these values remained many orders of magnitude higher than values previously reported in the literature [63]. Figure 4.3 displays the permeability values corresponding to the uncharacteristically high volumetric flow rates.

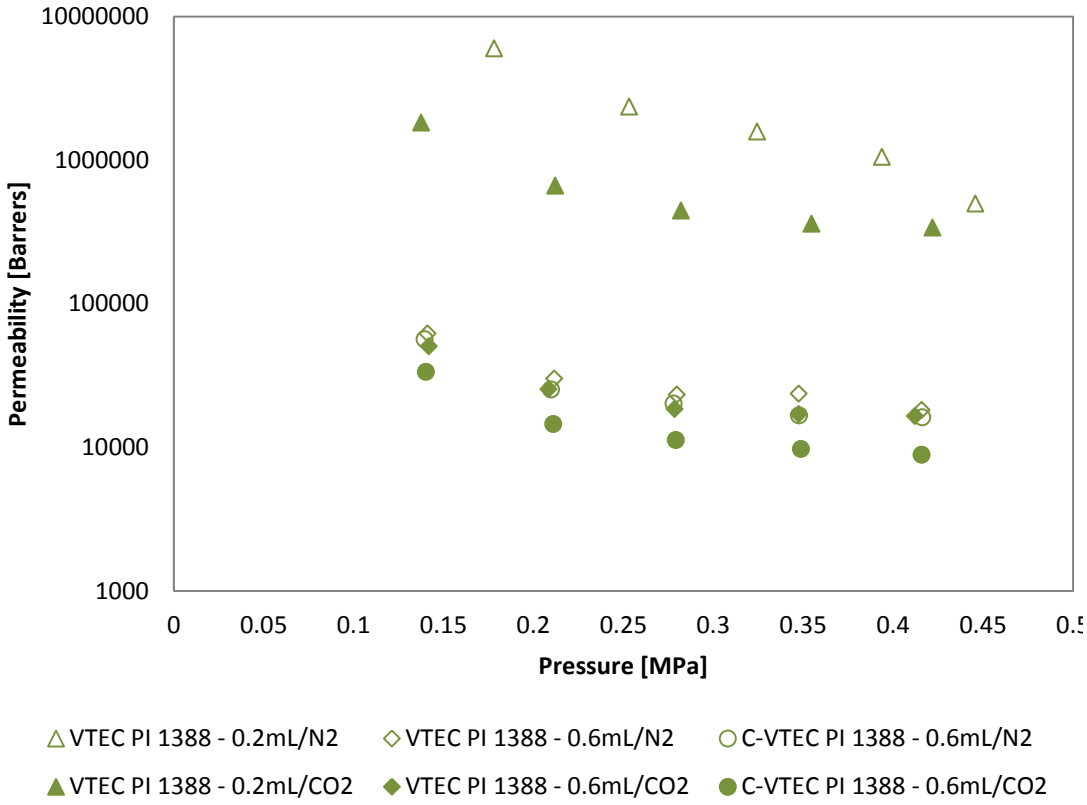

Figure 4.3: Average VTEC PI 1388 gas permeability indicative of MVs

Flow rates and corresponding permeabilites above or equal to those displayed in Figure 4.2 and Figure 4.3 respectively, are key initial indicators that gas is bypassing the membrane filter either through unsealed MVs or due to membrane failure. Membranes below approximately 10 µm in thickness were inherently more difficult to repair and tended to fail while being tested in the MTU as soon as a pressure differential was applied. After testing hundreds of membranes with thicknesses ranging from approximately 530 µm to 5 µm, an optimal thickness of approximately 10 µm was selected as being the thinnest membrane able to support itself within the MTU and, when

created using 0.6 mL of polymer solution, was able to maintain a very low concentration of visible MVs.

4.1.2 PBI Processing Results

For the PBI membranes, 10 μm was also targeted as the desired thickness for testing purposes. Initially, with 0.2 mL applied to the glass substrate (30 sec spin time), a large range of thicknesses were able to be achieved over spin rates from 500 to 900 rpm. By increasing the applied volume to 0.4 mL and the spin time from 35 to 45 sec, the thicknesses were able to be controlled closer to the target. These relationships are displayed in Figure 4.4.

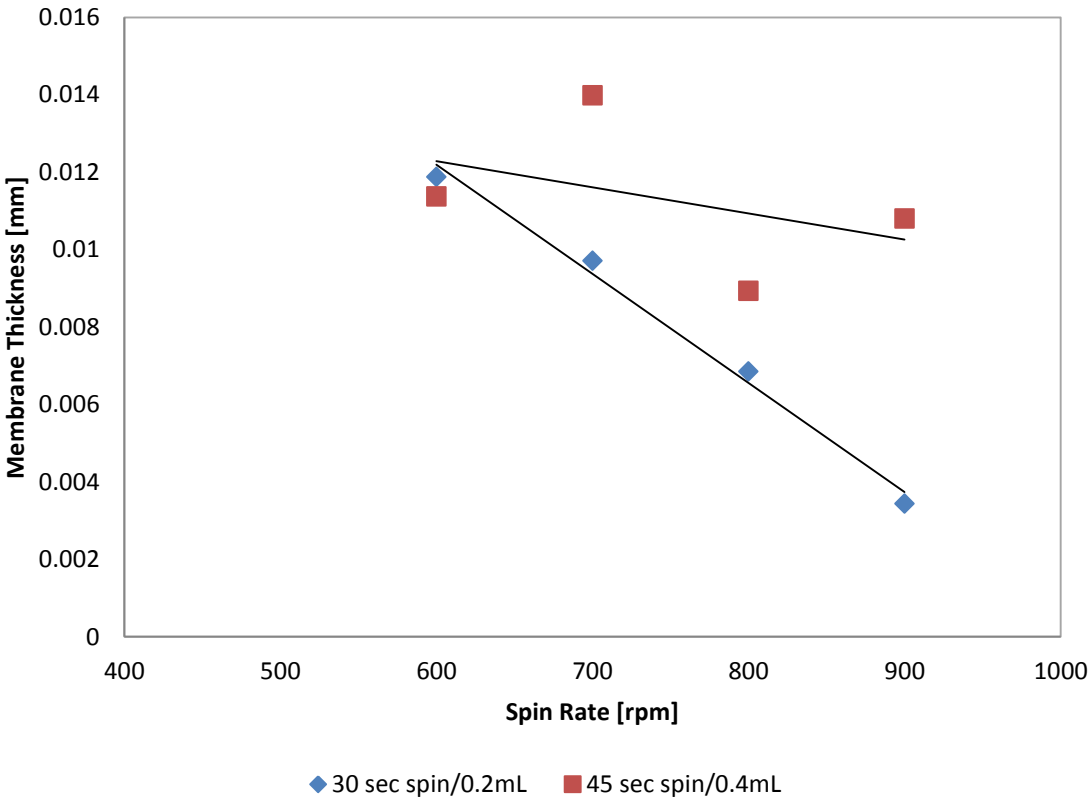

Figure 4.4: Average PBI membrane thickness for given spin rates

A smaller number of PBI membranes were needed to discover the target thickness settings that produced a low concentration of MV's as similar methods to the VTEC process were applied. The PBI was however, more brittle after being processed and proved more difficult to successfully remove from the substrate without damaging the integrity of the membrane. As a result, fewer gas flow trials could be accomplished. When the flow rates experienced were indicative of MVs (similar to those presented in Figure 4.2) the experiment was aborted.

4.1.3 DOP/PVC Processing Results

Similar to the separating membranes, a target thickness of 10 μm was selected for the caulking layer to insure that the entire separating membrane surface was covered and all MV's were blocked sufficiently. In selecting the concentration of DOP to mix with the PVC, the caulking membranes were inspected separately from their separating counter parts.

The 20 w/w% DOP/PVC membranes were unable to have more than 0.2 mL applied to the substrate prior to spinning due to the low viscosity of the mixture. The final cast membranes for this concentration did not consistently remain attached to the separating membrane and did not always maintain structural stability. The 60 w/w% DOP/PVC membranes, once cast, were very glassy in nature. They did not consistently adhere to the separating membrane which indicates that they were not sealing the MV's present in the separating layer. Each of the 30, 40, and 50 w/w% DOP/PVC produced sufficiently rubbery membranes that seemed to adhere to the separating layer without issue. Further investigation of the 40 w/w% DOP/PVC mixture was undertaken as it was

the middle ground between the 20 and 60 w/w% extremes. Figure 4.5 displays the full thickness characterization that was performed on the 40 w/w% mixture between 500 and 1200 rpm to determine the optimal spin rate to produce the target 10 µm caulking membrane.

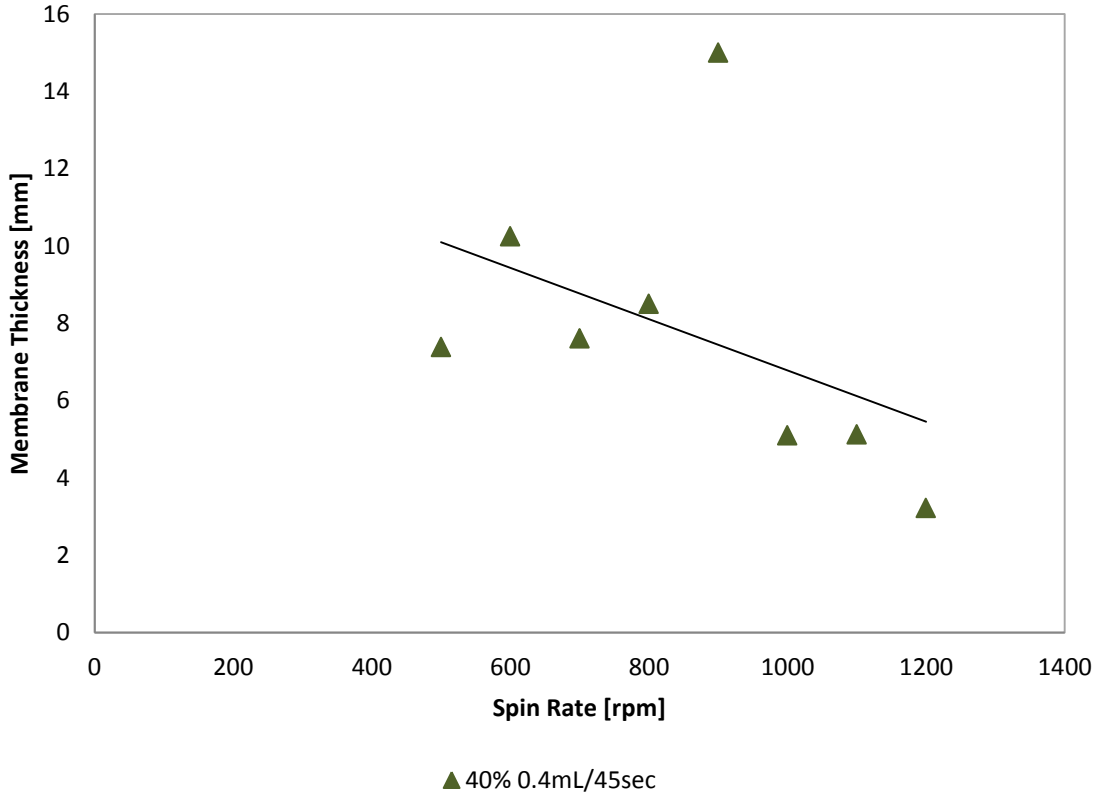

Figure 4.5: Spin rate vs. thickness characterization for 40% DOP/PVC caulking mixture

Figure 4.5 indicates that spin rates of 500 rpm or lower will produce membranes of approximately 10 µm. The outlying point at 900 rpm may have been due to other particles drying to either the separating membrane or the caulking membrane during the curing process.

4.2 Volumetric Gas Flow Characterization Results

Permeabilities below 1000 Barrers were able to be achieved using the 0.6 mL applied polymer volume for VTEC PI 1388 and 0.4 mL applied polymer volume for PBI both with 45 sec spin times with the caulking layer applied. Corresponding separating layer membrane thicknesses for the DOP/PVC coated VTEC PI 1388 and PBI were 8.75 μm and 8.25 μm respectively. In comparing the CO_2 and N_2 permeabilities of the trials that did not indicate MVs for the non-caulked membranes with the caulked membranes, very little difference was observed. This indicates that the intrinsic permeability of the VTEC PI 1388 for the given surface area and membrane thickness was being measured (see Figure 4.6) and was unaffected by the DOP/PVC caulking material. Measuring the 4 quadrants of the membrane and caulking material layers and averaging the thicknesses, while it is still attached to the glass substrate, does provide a reliable thickness measurement of each layer. When spun, the membrane and caulking material layers are close to being uniform and thus the averaging applied can be used to assume a flat feed stream interface.

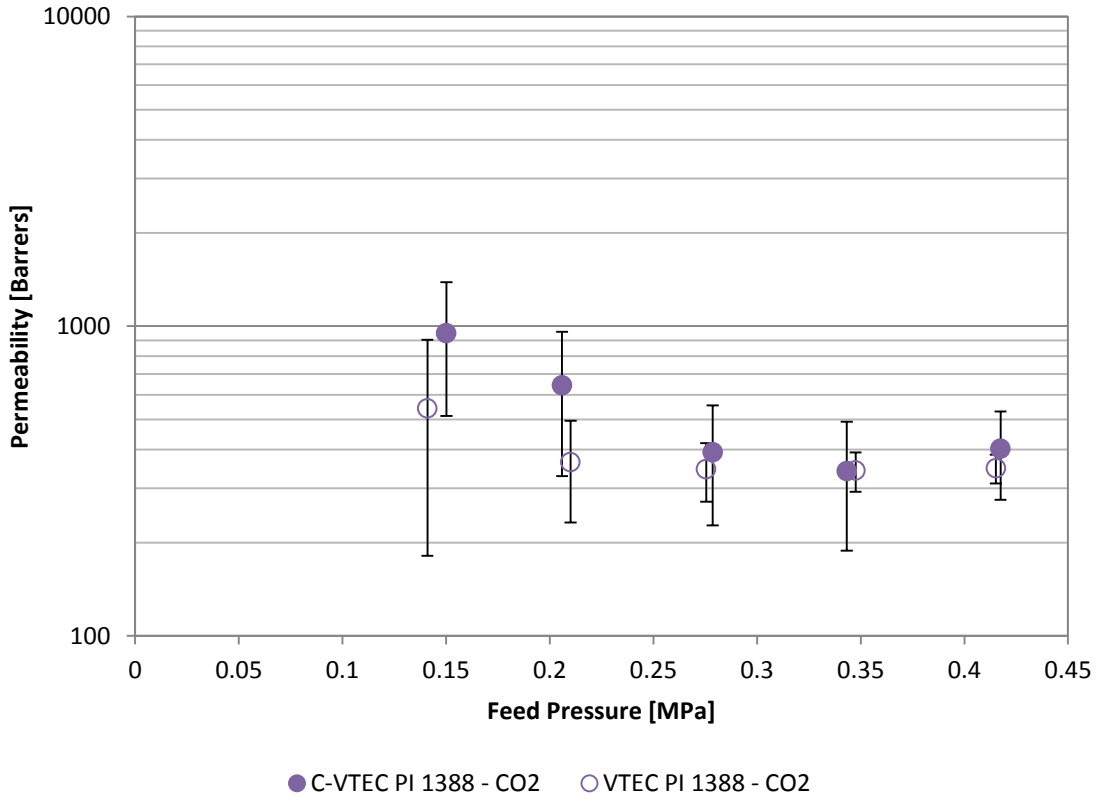

Figure 4.6: CO_2 permeability for DOP/PVC caulked and un-caulked VTEC PI 1388

The trend observed in the data indicates a decrease in permeability as the pressure is increased at approximately 25°C. The change in permeability between data points diminishes as feed pressure is increased, indicating that at higher pressures, the permeability values would be similar. A smaller standard deviation can also be observed at higher feed pressures, likely due to the amount of compression experienced by the DOP/PVC coating which also indicates a trend toward a uniform value. The final average data points corresponding to the highest tested pressure for both caulked and un-caulked VTEC PI 1388 shows a slight increase in permeability. However, the trend lies within the standard deviation of this point and it is expected that at higher feed pressures, a uniform

permeability would be maintained. The error bars in Figure 4.6 represent one standard deviation of the permeability values at each pressure with the same membrane. As each membrane was exposed to the set pressures in ascending order a total of four times prior to the gas being changed, membrane hysteresis may be responsible for the upward trend in permeability for the higher pressures.

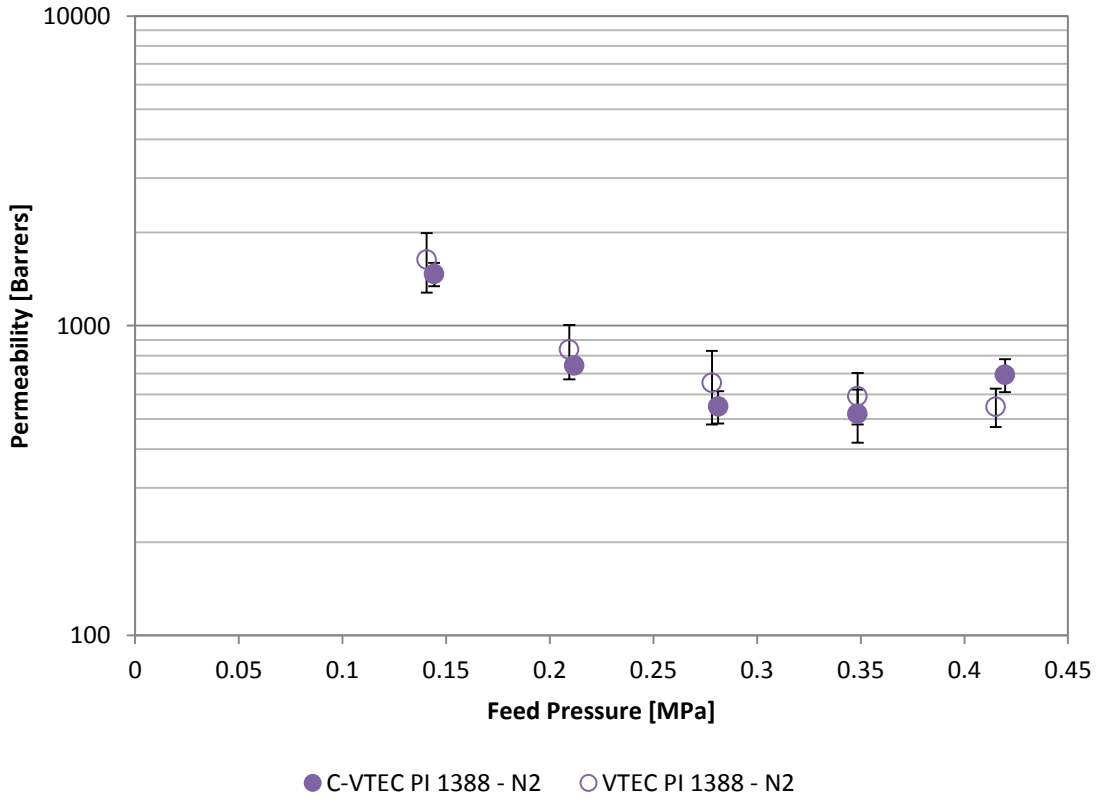

Figure 4.7: N_2 permeability for DOP/PVC caulked and un-caulked VTEC PI 1388

Nitrogen experienced less of a difference between the caulked and un-caulked membranes. This is indicative of a higher permeability to N_2 expressed by both the DOP/PVC and VTEC PI 1388 membranes at 25°C. The error bars in Figure 4.7 again represent the standard deviation of the permeability values at each pressure experienced

by the same membrane across multiple trials. The upward trend at the higher set pressures may again be due to the cycling of a single membrane for each set of trials for this gas.

The volumetric gas flow rates that were measured during testing of intact caulked membranes of both the PBI and the VTEC PI 1388 are displayed in Figure 4.8.

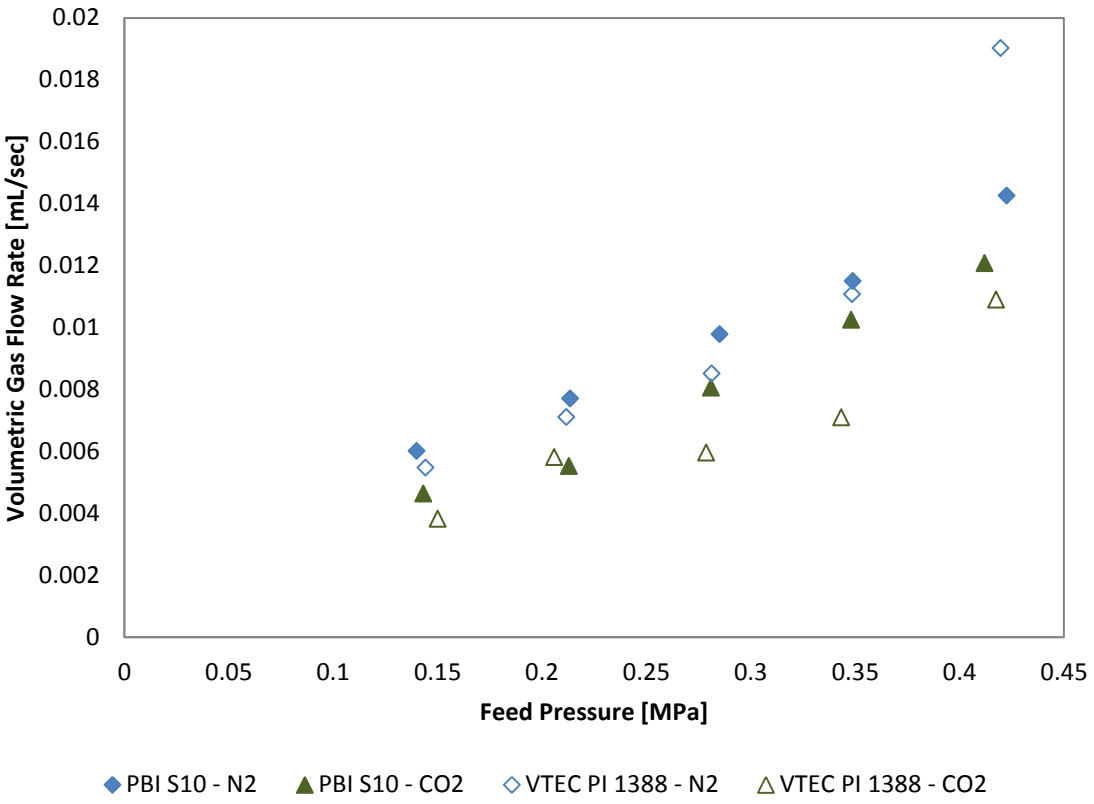

Figure 4.8: Caulked PBI S10 and VTEC PI 1388 average volumetric gas flow rates using CO_2 and N_2

A positive linear correlation exists between the feed pressure and the volumetric gas flow rate. The volumetric gas flow rates for the trials where MVs were absent displayed rates that were approximately 50-60% lower than the slowest flowing trials where MVs were

determined to be present. Both the caulked PBI and the caulked VTEC PI 1388 had very similar gas flow rates for both the CO_2 and N_2 trials.

The gas permeabilities experienced during the successful trials where MVs were absent and/or sealed by the caulking membrane were low compared to all other trials. The permeabilities displayed in Figure 4.9 can therefore be considered the intrinsic gas permeabilities for the given feed pressures, membrane thicknesses, and polymer type at 25°C.

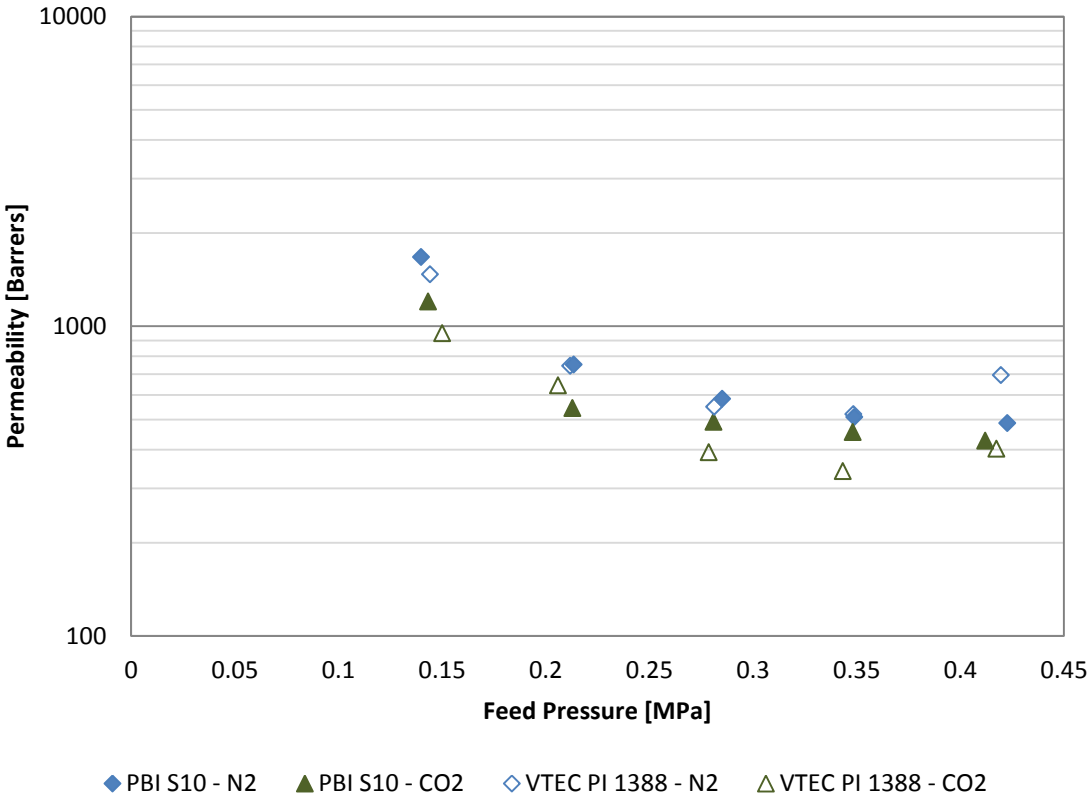

Figure 4.9: PBI S10 and VTEC PI 1388 permeability to CO_2 and N_2

A decreasing trend in the permeability can be observed with increasing feed pressure. At the higher pressures the permeability stabilizes indicating that the membrane's network of folded polymer chains has fully compressed. As permeability is inversely proportional to the difference in pressure across the membrane, the results indicate that the pressure effects are becoming less impactful as the feed pressure is increased and that the effect of volumetric gas flow rate begins to govern the resulting permeability at these higher pressures.

The permselectivity for CO_2 over N_2 was below 1.0 for both the PBI and the VTEC PI 1388 membranes. This indicates that both will favour N_2 over CO_2 under the conditions investigated (see Figure 4.10).

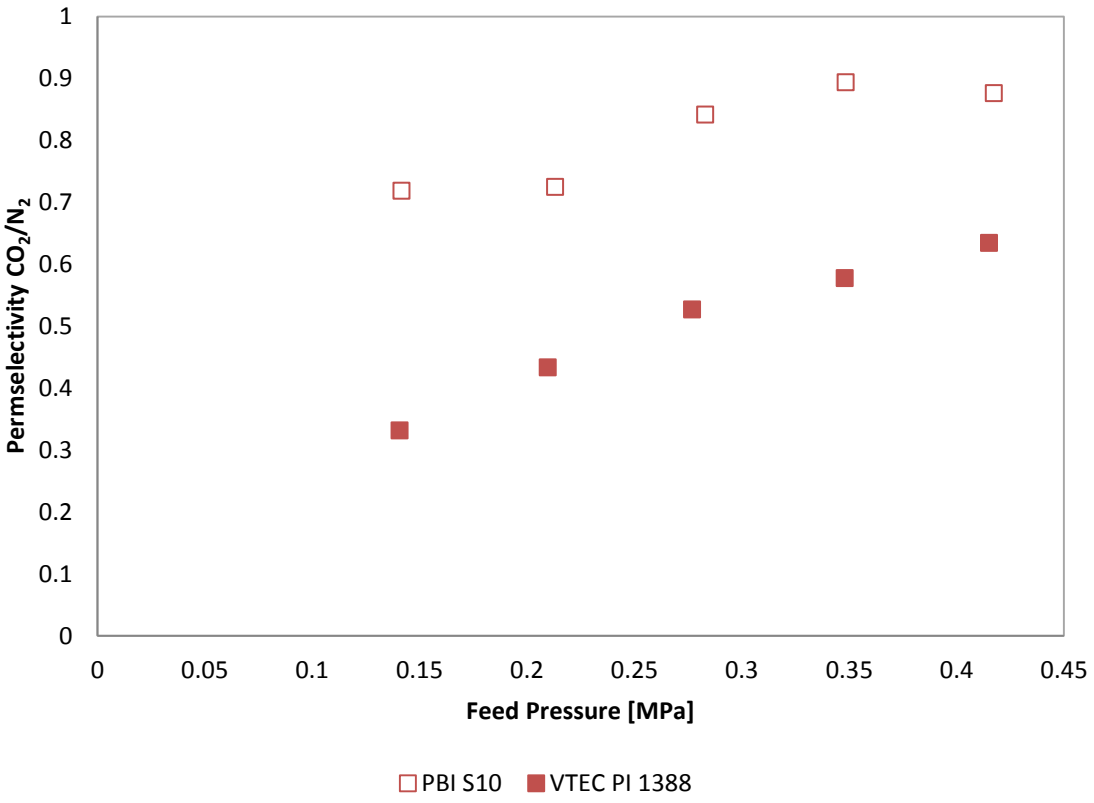

Figure 4.10: CO_2/N_2 Permselectivity for VTEC PI 1388 and PBI

The permselectivity of the PBI and the VTEC PI 1388 both tended toward being more selective for CO_2 as pressure was increased. In comparing the two membranes, the filtration of CO_2 is less favoured in the VTEC PI 1388 membrane. Both data sets, like the corresponding permeabilities are trending toward a uniform value for permselectivity. This value will likely be realized at much higher pressures than those tested here.

The temperatures, across all VTEC PI 1388 and PBI trials were maintained between 24.2±0.8 °C. Variation of the set pressure for trials targeted at 20, 30, 40, 50, and 60 psi were 20.8±1.5, 30.8±2.9, 40.8±2.1, 51.0±2.2, and 60.8±1.9 psi.

4.3 Discussion

The physiochemical properties that affect the intrinsic properties of the final membrane are well understood. However, current models only conform to empirical data and are not able to predict transport behaviour of membranes formed from newly discovered polymers or those that are outside of the data set used to create these correlations. Non-ideal module flow patterns and membrane separating layer imperfections have been cited to affect the selectivity of the actual operating membrane compared to the ideal values obtained through modeling [18]. While the models presented in this research are a good tool for reducing the number of potential polymer candidates for a given membrane separation process, very specific information on the operating requirements of the membrane needs to be understood prior to final selection. Membranes may be favoured based on controlled bench top trials, but may have qualities that are vastly over or under the necessary requirements for the given application.

The intrinsic permeabilities of PBI and VTEC PI 1388 were analysed using both coated and uncoated dense polymeric membranes. The results indicated that in the coated membranes, the permeabilities were very similar. Processing methods for membrane fabrication improved throughout the project to a point where creating a higher ratio of successful to unsuccessful thin membranes was achieved. The permeabilities of CO_2 and N_2 for both VTEC PI 1388 and PBI remained higher than values reported in the literature. However, many of these reports failed to mention either temperature or pressure conditions under which the membranes were tested as well as the membrane thickness used for data collection. The methods for creating the polymer solutions, heat treatment

of the membranes, and testing methods also seemed to vary between authors. This is an indication that the conditions under which the trials presented in this report were completed, yielded accurate permeabilities for VTEC PI 1388 and PBI specific to the methods used.

Spin coating of polymers prior to applying a temperature based phase inversion process is a novel processing method directed specifically at small scale membranes. This method is not widely explored in the membrane literature as industrial GS applications generally require a large surface area for economical filtration and spin coaters of that magnitude do not exist. This processing method may have led to larger intersegmental spacing of polymer back bone chains (*i.e.* a larger FFV) due to the centrifugal forces applied during the spin coat process. The result of applying the spin coating method is that membrane thicknesses were able to be controlled using an empirical linear correlation between spin rate, spin duration, and volume of polymer solution applied to the substrate rather than employing complicated predictive methods presented by Emslie et al. ([66]) as well as Yonkoski and Soane ([67]) .

As the tested polymers were also commercially purchased batch preparation methods, solvent concentration, and polymer dissolution may have varied between production runs causing differences to arise when comparing to older published data. The permeability and permselectivity data acquired in this investigation was from the same batches of polymer solution indicating that variations experienced during these trials were due to the presence of pin holes or MVs that were unable to be sealed by the repair procedure presented in Section 3.3.

Chapter 5: Conclusions and Future Recommendations

5.1 Conclusions

The permselectivities of the membranes, created using the spin coating method, for both VTEC PI 1388 and PBI membranes were not in favour of CO_2 for any of the pressure differences investigated. This indicates that these membranes should not be used in compartmental CO_2 sensing applications as confounding gas permeants, specifically N_2, will interfere with the sensor, especially if non-selective sensing methods are employed.

The pure gas permeability for five set pressures of CO_2 and N_2 through spin coated VTEC PI 1388 and PBI at 24.2±0.8 °C was determined. For CO_2 and N_2 moving through VTEC PI 1388, the permeability coefficient varied from 540±360 to 340±37 Barrers and from 1600±350 to 540±77 Barrers for feed pressures from 0.14 to 0.41 MPa respectively. For CO_2 and N_2 moving through PBI, the permeability coefficient varied from 1200±98 to 400±8.6 Barrers and from 1670±160 to 480±21 Barrers for feed pressures from 0.14 to 0.41 MPa respectively. The corresponding permselectivities for CO_2/N_2 for VTEC PI 1388 and PBI ranged from 0.33 to 0.63 and 0.72 to 0.87 for feed pressures from 0.14 to 0.41 MPa respectively.

The ability of the glassy membranes selected for this analysis to filter larger particulate matter or gases with larger kinetic diameters remains intact. As the methods presented here to form, spin-coat, and repair membranes have been refined to the point where larger quantities of membranes can be created, repaired, and tested in a short

period of time, investigation into various other commercially available membranes can be accomplished.

5.2 Recommendations

Four variables were uncovered in this research that may have an effect on the intrinsic filtration properties of the membrane and should be investigated further to fully quantify those effects, they are:

- Initial polymer material choice based on side-chain inhibition of back-bone rotation and packing;
- Feed and permeate stream pressures and temperatures;
- Membrane casting methods;
- Membrane curing methods;

Most notable of these variables is the initial polymer material choice. While material selection can be based on permeabilities reported in the literature, a polymer able to filter different phases of a substance has not been reported. A small investigation on feed stream pressures was undertaken in this study for the VTEC PI 1388 and PBI membranes within the gas region of these gases, but further understanding can be gained from controlling the permeate stream pressure as well. By controlling the pressure differential, rather than just the feed stream pressure, insight into the filtering properties of the membrane for permeates in different states can be gained. With the ultimate goal being to use a membrane in conjunction with a CO_2 sensor that may be required to detect

various states of CO_2 under geologic storage conditions, this type of study would be beneficial to determine the operating range of the sensor.

Forming a basis of permeability data using the testing conditions (in terms of pressure and temperature) most like the ones expected in the sensing environment, allows for beneficial modifications to be explored that could further enhance permeability and permselectivity for CO_2 over any number of gases. Structural changes in the polymer backbone such as the substitution of less bulky groups with larger groups tend to open the matrix, increase the resistance to motion at rotational joints of the polymer back bone and may be the most effective way to increase permeability to specific permeants without causing large drops in selectivity [17]. Side chain modification should target both the inhibition of the intersegmental packing of the polymer backbone and the degree of intrasegmental mobility, or amount of backbone rotation. Bulky phenyl groups specifically, increase intersegmental attractions to offset some of the increase in spacing [17]. However, in selecting an appropriate side-chain addition or substitution, details of the chemical structure must be known for successful modification to occur. For that reason, it is not recommended to pursue VTEC PI polymers for modifications in this regard, rather investigate other VTEC blends for intrinsic properties that may favour CO_2 separation under the target conditions.

It is understood that for most applications in which a supercritical fluid is being separated, solubility selectivity based selection of polymer material is not attractive. Structural modifications of glassy membranes in particular that may enhance gas solubility selectivity can actually lead to excessive swelling of the membrane when

supercritical fluids are involved, leading to overall losses to molecular mobility [18]. Therefore, one should focus on modifications that enhance the diffusivity instead.

There are many ways to create a flat, thin membrane and there are no studies in the literature that compare the effects that the casting methods, curing temperatures and pressures, or the curing environment have on the filtering properties of a specific membrane. Spin-coating the polymer film onto the substrate may cause an increase in intrinsic permeability of gases by causing less polymer backbone entanglement to occur. This may be a result of the centripetal forces pulling the polymer to the outer rim of the substrate. The lower level of backbone entanglement acts to increase the membrane's FFV leading to lower selectivities for select gases. For shorter duration spins, a higher density of backbone entanglement may be found closer to the outer edge of the substrate, however the extent of this build up was not measured in this analysis and further investigation into this phenomenon and its impact on the permeability of a given membrane needs further investigation.

Good improvements in permeability have been shown for CO_2/CH_4 and CO_2/H_2 separations after the membranes underwent long-period heat treatments in an effort to remove all remaining water and organic solvent from the polymer matrix [63]. Water entrapped within a polymer matrix, either through physisorption from the surroundings or from an incomplete film processing, can cause selectivities and fluxes to change dramatically [15]. A study involving both the effect of selected casting method and curing temperature/duration would improve the understanding of the interplay between these variables and how they modify the permeability/permselectivity relationship for

membranes intended for sensor applications. To make measurements of the intrinsic properties of polymer membranes that are more consistently accurate, a much higher level of control of feed and permeate pressures and temperatures, membrane thicknesses, membrane surface uniformity, and duration of atmospheric exposure prior to testing needs to be undertaken.

Bibliography

[1] M. Mulder, *Basic Principles of Membrane Technology*. Kluwer Academic Publishers, 1992.

[2] W. J. J. Huijgen, "Carbon dioxide sequestration by mineral carbonation," 2003.

[3] J. L. Lewicki, "An improved strategy to detect CO 2 leakage for verification of geologic carbon sequestration," *Geophys. Res. Lett.*, vol. 32, no. 19, p. L19403, 2005.

[4] R. Giese, J. Henninges, S. Lüth, D. Morozova, C. Schmidt-Hattenberger, H. Würdemann, M. Zimmer, C. Cosma, and C. Juhlin, "Monitoring at the CO2 SINK site: A concept integrating geophysics, geochemistry and microbiology," *Energy Procedia*, vol. 1, no. 1, pp. 2251–2259, Feb. 2009.

[5] T. Gentzis, "Subsurface sequestration of carbon dioxide — an overview from an Alberta (Canada) perspective," *Int. J. Coal Geol.*, vol. 43, no. 1–4, pp. 287–305, 2000.

[6] L. Andre, P. Audigane, M. Azaroual, and a Menjoz, "Numerical modeling of fluid–rock chemical interactions at the supercritical CO2–liquid interface during CO2 injection into a carbonate reservoir, the Dogger aquifer (Paris Basin, France)," *Energy Convers. Manag.*, vol. 48, no. 6, pp. 1782–1797, Jun. 2007.

[7] C. M. Oldenburg, K. Pruess, and S. M. Benson, "Process Modeling of CO2 Injection into Natural Gas Reservoirs for Carbon Sequestration and Enhanced Gas Recovery," *Energy*, vol. 22, no. 6, pp. 293–298, 2001.

[8] Z. Duan, N. Møller, and J. H. Weare, "An equation of state for the CH4-CO2-H2O system: I. Pure systems from 0 to 1000°C and 0 to 8000 bar," *Geochim. Cosmochim. Acta*, vol. 56, no. 7, pp. 2605–2617, Jul. 1992.

[9] Z. Duan, N. Møller, and J. H. Weare, "An equation of state for the CH4-CO2-H2O system: II. Mixtures from 50 to 1000°C and 0 to 1000 bar," *Geochim. Cosmochim. Acta*, vol. 56, no. 7, pp. 2619–2631, Jul. 1992.

[10] Z. Duan and R. Sun, "An improved model calculating CO2 solubility in pure water and aqueous NaCl solutions from 273 to 533 K and from 0 to 2000 bar," *Chem. Geol.*, vol. 193, no. 3–4, pp. 257–271, Feb. 2003.

[11] J. I. Yuanhui, J. I. Xiao, L. I. U. C. I, and L. U. Linghong, "Progress in the Study on the Phase Equilibria of the C02-H20 and Systems," *Chinese J. Chem. Eng.*, vol. 15, no. 3, pp. 439–448, 2007.

[12] C. Ukaegbu, O. Gundogan, E. Mackay, G. Pickup, a Todd, and F. Gozalpour, "Simulation of CO_2 storage in a heterogeneous aquifer," *Proc. Inst. Mech. Eng. Part A J. Power Energy*, vol. 223, no. 3, pp. 249–267, May 2009.

[13] D. Li and Z. Duan, "The speciation equilibrium coupling with phase equilibrium in the H2O–CO2–NaCl system from 0 to 250°C, from 0 to 1000 bar, and from 0 to 5 molality of NaCl," *Chem. Geol.*, vol. 244, no. 3–4, pp. 730–751, Oct. 2007.

[14] L. Marini, *Geological Sequestration of Carbon Dioxide: Thermodynamics, kinetics, and reaction path modeling*, 11th ed., no. I. Amsterdam, The Netherlands: Elseiver B. V., 2007, p. 453.

[15] S. T. Oyama and S. M. Stagg-Williams, Eds., *Inorganic, Polymeric and Composite Membranes: Structure, Function, and Other Correlations*, 14th ed. Elseiver B. V., 2011.

[16] L. M. Robeson, "Correlation of Separation Factor Versus Permeability for Polymeric Membranes," *J. Memb. Sci.*, vol. 62, no. 2, pp. 165–185, 1991.

[17] W. J. Koros, G. K. Fleming, S. M. Jordan, T. H. Kim, and H. H. Hoehn, "Polymeric Membrane Materials for Solution-Diffusion Based Permeation Separations," *Prog. Polym. Sci.*, vol. 13, no. 4, pp. 339–401, 1988.

[18] W. J. Koros and G. K. Fleming, "Membrane-Based Gas Separation," *J. Memb. Sci.*, vol. 83, pp. 1–80, 1993.

[19] R. W. Baker, *Membrane Technology and Applications*. Chichester, UK: John Wiley & Sons, Ltd, 2012.

[20] T. Xu, Ed., *Advances in Membrane Science and Technology*. Nova Science Publishers, Inc., 2009.

[21] A. Fick, "On liquid diffusion," *J. Memb. Sci.*, vol. 100, no. 1, pp. 33–38, Mar. 1995.

[22] S.-T. Hwang, "Fundamentals of membrane transport," *Korean J. Chem. Eng.*, vol. 28, no. 1, pp. 1–15, Dec. 2010.

[23] J. G. Wijmans and R. W. Baker, "The solution-diffusion model: a review," *J. Memb. Sci.*, vol. 107, no. 1–2, pp. 1–21, Nov. 1995.

[24] S.-T. Hwang, “Nonequilibrium thermodynamics of membrane transport,” *AIChE J.*, vol. 50, no. 4, pp. 862–870, Apr. 2004.

[25] C. Charcosset, “Chapter 1: Principles on Membrane and Membrane Processes,” in *Membrane Processes in Biotechnologies and Pharmaceutics*, no. c, Elsevier Science and Technology Books, Inc., 2012.

[26] I. Pinnau and B. D. Freeman, “Formation and Modification of Polymeric Membranes: Overview,” in *Membrane Formation and Modification*, Menlo Park, CA: Membrane Technology and Research, Inc., 2000, pp. 1–22.

[27] C. J. M. van Rijn, Ed., *Nano and Micro Engineered Mebrane Technology*, 1st ed. Elsevier B.V., 2004.

[28] S. P. Nunes and K. V. Peinemann, Eds., *Membrane Technology in the Chemical Industry*, 2nd, rev. . Wiley-VCH, 2006.

[29] X. Zhang, Y. Chen, A. H. Konsowa, X. Zhu, and J. C. Crittenden, “Evaluation of an innovative polyvinyl chloride (PVC) ultrafiltration membrane for wastewater treatment,” *Sep. Purif. Technol.*, vol. 70, no. 1, pp. 71–78, Nov. 2009.

[30] R. Abedini and A. Nezhadmoghadam, “Application of Membrane in Gas Separation Processes: Its Suitaility and Mechanisms,” *Pet. Coal*, vol. 52, no. 2, pp. 69–80, 2010.

[31] Y. Yompolskii, I. Pinnau, and B. D. Freeman, Eds., *Materials Science of Membranes for Gas and Vapor Separation*. John Wiley & Sons, Ltd, 2006.

[32] R. J. R. Uhlhorn, K. Keizer, and A. J. Burggraaf, “Gas and Surface Diffusion in Modified γ-Alumina Systems,” *J. Memb. Sci.*, vol. 46, pp. 225–241, 1989.

[33] D. F. Sanders, Z. P. Smith, R. Guo, L. M. Robeson, J. E. McGrath, D. R. Paul, and B. D. Freeman, “Energy Efficient Polymeric Gas Separation Membranes for a Sustainable Future: A Review,” *Polymer (Guildf).*, Jul. 2013.

[34] C. E. Powell and G. G. Qiao, “Polymeric CO2/N2 gas separation membranes for the capture of carbon dioxide from power plant flue gases,” *J. Memb. Sci.*, vol. 279, no. 1–2, pp. 1–49, Aug. 2006.

[35] Y. Shangguan, “Intrinsic Properties of Poly(Ether-B-Amide) (Pebax®1074) for Gas Permeation and Pervaporation,” 2011.

[36] V. E. Ryzhikh, a. Y. Alent’ev, and Y. P. Yampol’skii, “Relation of gas-transport parameters of amorphous glassy polymers to their free volume: Positron annihilation study,” *Polym. Sci. Ser. A*, vol. 55, no. 4, pp. 244–252, Apr. 2013.

[37] S. Sugden, “Molecular Volumes at Absolute Zero. Part II. Zero Volumes and Chemical Composition,” *J. Chem. Soc.*, pp. 1786–1798, 1927.

[38] A. Bondi, “van der Waals Volumes and Radii,” *J. Phys. Chem.*, vol. 68, no. 3, pp. 441–451, 1964.

[39] J. Y. Park and D. R. Paul, “Correlation and prediction of gas permeability in glassy polymer membrane materials via a modified free volume based group contribution method,” *J. Memb. Sci.*, vol. 125, pp. 23–39, Mar. 1997.

[40] D. Shekhawat, D. R. Luebke, and H. W. Pennline, “A Review of Carbon Dioxide Selective Membranes,” 2003.

[41] L. M. Robeson, W. F. Burgoyne, M. Langsam, A. C. Savoca, and C. F. Tien, “High Performance Polymers for Membrane Separation,” *Polymer (Guildf).*, vol. 35, no. 23, pp. 4970–4978, 1994.

[42] K. Toi, G. Morel, and D. R. Paul, “Gas Sorption and Transport in Poly(phenylene Oxide) and Comparisons with Other Glassy Polymers,” *J. Appl. Polym. Sci.*, vol. 27, pp. 2997–3005, 1982.

[43] C. L. Liou, L. a. Wang, and M. C. Shih, “Characteristics of hydrogenated fiber Bragg gratings,” *Appl. Phys. A Mater. Sci. Process.*, vol. 64, no. 2, pp. 191–197, Jan. 1997.

[44] B. D. Freeman, “Basis of Permeability/Selectivity Tradeoff Relations in Polymeric Gas Separation Membranes,” *Macromolecules*, vol. 32, pp. 375–380, 1999.

[45] W. W. Brandt, “Model Calculation of the Temperature Dependence of Small Molecule Diffusion in High Polymers,” *J. Phys. Chem.*, vol. 63, no. 7, pp. 1080–1085, 1959.

[46] R. M. Barrer and G. Skirrow, “Transport and equilibrium phenomena in gas-elastomer systems. I. Kinetic phenomena,” *J. Polym. Sci.*, vol. 3, no. 4, pp. 549–563, 1948.

[47] D. W. van Krevelen and K. te Nijenhius, *Properties of Polymers- Their Correlation with Chemical Structure; Their Numerical Estimation and Prediction from Additive Group Contributions*, 4th ed. Elsevier Science, 2009.

[48] Y. Yampolskii, S. Shishatskii, A. Alentiev, and K. Loza, “Correlations with and prediction of activation energies of gas permeation and diffusion in glassy polymers,” *J. Memb. Sci.*, vol. 148, no. 1, pp. 59–69, Sep. 1998.

[49] A. Y. Alentiev and Y. P. Yampolskii, “Free volume model and tradeoff relations of gas permeability and selectivity in glassy polymers,” *J. Memb. Sci.*, vol. 165, no. 2, pp. 201–216, Feb. 2000.

[50] Y. H. Zhao, M. H. Abraham, and A. M. Zissimos, “Fast calculation of van der Waals volume as a sum of atomic and bond contributions and its application to drug compounds.,” *J. Org. Chem.*, vol. 68, no. 19, pp. 7368–73, Sep. 2003.

[51] L. M. Robeson, C. D. Smith, and M. Langsam, “A group contribution approach to predict permeability and permselectivity of aromatic polymers,” vol. 132, pp. 33–54, 1997.

[52] L. M. Robeson, “The Upper Bound Revisited,” *J. Memb. Sci.*, vol. 320, no. 1–2, pp. 390–400, Jul. 2008.

[53] P. Bernardo, E. Drioli, and G. Golemme, “Membrane Gas Separation: A Review/State of the Art,” *Ind. Eng. Chem. Res.*, vol. 48, no. 10, pp. 4638–4663, May 2009.

[54] Y. Yampolskii, “Polymeric Gas Separation Membranes,” *Macromolecules*, vol. 45, pp. 3298–3311, 2012.

[55] D. R. Pesiri, B. Jorgensen, and R. C. Dye, “Thermal optimization of polybenzimidazole meniscus membranes for the separation of hydrogen, methane, and carbon dioxide,” *J. Memb. Sci.*, vol. 218, pp. 11–18, Jul. 2003.

[56] P. Tiemblo, J. Guzmán, E. Riande, C. Mijangos, and H. Reinecke, “The Gas Transport Properties of PVC Functionalized with Mercapto Pyridine Groups,” *Macromolecules*, vol. 35, no. 2, pp. 420–424, Jan. 2002.

[57] E. Riande, C. Mijangos, H. Reinecke, P. Tiemblo, and J. Guzma, “Effect of physical aging on the gas transport properties of PVC and PVC modified with pyridine groups,” vol. 42, pp. 4817–4823, 2001.

[58] K. Bierbrauer, M. López-González, E. Riande, and C. Mijangos, “Gas transport in fluorothiophenyl modified PVC membranes,” *J. Memb. Sci.*, vol. 362, no. 1–2, pp. 164–171, Oct. 2010.

[59] C. a. Jones, S. a. Gordeyev, and S. J. Shilton, “Poly(vinyl chloride) (PVC) hollow fibre membranes for gas separation,” *Polymer (Guildf).*, vol. 52, no. 4, pp. 901–903, Feb. 2011.

[60] C. Lim, C. Kim, W. Kim, Y. Jeong, and Y. Lee, “Gas Permeable Membranes Composed of Carboxylated Poly (vinyl chloride) and Polyurethane,” *Bull. Korean Chem. Soc.*, vol. 20, no. 6, pp. 672–676, 1999.

[61] I. Hamerton, “High-Performance Thermoset-Thermoset Polymer Blends: A Review of the Chemistry of Cyanate Ester-Bismaleimide Blends,” *High Perform. Polym.*, vol. 8, pp. 83–95, 1996.

[62] H. Vogel and C. S. Marvel, “Polymenzimidazoles, New Thermally Stable Polymers,” *J. Polym. Sci.*, vol. 50, pp. 511–539, 1961.

[63] J. R. Klaehn, C. J. Orme, E. S. Peterson, T. A. Luther, M. G. Jones, A. K. Wertshing, and J. M. Urban-Klaehn, “CO2 Separation Using Thermally Optimized Membranes : A Comprehensive Project Report (2000 – 2007),” 2008.

[64] S. H. Han, J. E. Lee, K.-J. Lee, H. B. Park, and Y. M. Lee, “Highly gas permeable and microporous polybenzimidazole membrane by thermal rearrangement,” *J. Memb. Sci.*, vol. 357, no. 1–2, pp. 143–151, Jul. 2010.

[65] R. E. Kesting, *Synthetic Polymeric Membranes: A Structural Perspective*, 2nd ed. New York: Wiley, 1985.

[66] A. G. Emslie, F. T. Bonner, and L. G. Peck, “Flow of a Viscous Liquid on a Rotating Disk,” *J. Appl. Phys.*, vol. 29, no. 5, p. 858, 1958.

[67] R. K. Yonkoski and D. S. Soane, “Model for spin coating in microelectronic applications,” *J. Appl. Phys.*, vol. 72, no. 2, p. 725, 1992.

[68] F. Kreith, J. H. Taylor, and J. P. Chong, “Heat and Mass Transfer from a Rotating Disk,” *J. Heat Transfer*, vol. 81, p. 95, 1958.

[69] J. M. S. Henis and M. K. Tripodi, “Composite Hollow Fiber Membranes for Gas Separation: the Resistance Model Approach,” *J. Memb. Sci.*, vol. 8, pp. 233–246, 1981.

[70] M. L. Davies, C. J. Hamilton, S. M. Murphy, and B. J. Tighe, “Polymer membranes in clinical sensor applications,” *Biomaterials*, vol. 13, no. 14, pp. 971–978, Jan. 1992.

[71] J. W. Severinghaus, “First electrodes for blood PO2 and PCO2 determination.,” *J. Appl. Physiol.*, vol. 97, no. 5, pp. 1599–600, Nov. 2004.

[72] S. R. Gambino, “Determination of Blood pCO2,” *Clin. Chem.*, vol. 7, no. 4, pp. 236–245, 1961.

[73] S. Schutting, S. M. Borisov, and I. Klimant, “Diketo-pyrrolo-pyrrole dyes as new colorimetric and fluorescent pH indicators for optical carbon dioxide sensors.,” *Anal. Chem.*, vol. 85, no. 6, pp. 3271–9, Mar. 2013.

[74] X. Xie and E. Bakker, “Non-Severinghaus potentiometric dissolved CO2 sensor with improved characteristics.,” *Anal. Chem.*, vol. 85, no. 3, pp. 1332–6, Feb. 2013.

[75] B. Bao, L. Melo, B. Davies, H. Fadaei, D. Sinton, and P. Wild, “Detecting Supercritical CO2 in Brine at Sequestration Pressure with an Optical Fiber Sensor.,” *Environ. Sci. Technol.*, Nov. 2012.

[76] J. Lin, “Recent development and applications of optical and fiber-optic pH sensors,” *Trends Anal. Chem.*, vol. 19, no. 9, pp. 541–552, Sep. 2000.

[77] C.-S. Chu and Y.-L. Lo, “Highly sensitive and linear optical fiber carbon dioxide sensor based on sol–gel matrix doped with silica particles and HPTS,” *Sensors Actuators B Chem.*, vol. 143, no. 1, pp. 205–210, Dec. 2009.

[78] C.-S. Chu and Y.-L. Lo, “Fiber-optic carbon dioxide sensor based on fluorinated xerogels doped with HPTS,” *Sensors Actuators B Chem.*, vol. 129, no. 1, pp. 120–125, Jan. 2008.

[79] H. Segawa, E. Ohnishi, Y. Arai, and K. Yoshida, “Sensitivity of fiber-optic carbon dioxide sensors utilizing indicator dye,” *Sensors Actuators B Chem.*, vol. 94, no. 3, pp. 276–281, Oct. 2003.

[80] M. B. Tabacco, M. Uttamlal, M. McAllister, and D. R. Walt, “An Autonomous Sensor and Telemetry System for Low-Level pCO2 Measurements in Seawater,” *Anal. Chem.*, vol. 71, no. 1, pp. 154–161, 1998.

[81] W. R. Browall, “Method for Sealing Breaches in Multi-Layer Ultrathin Membrane Composites,” 3,980,4561976.

[82] V. P. Kharea, A. R. Greenberga, J. Zartmana, W. B. Krantzb, and P. Todd, “Macrovoid Growth During Polymer Membrane Casting,” *Desalination*, vol. 145, pp. 17–23, 2002.